

Near-infrared spectroscopy of nearby Seyfert galaxies. II. Molecular content and coronal emission

J. Reunanen¹, J.K. Kotilainen¹, M.A. Prieto^{2,3}

¹ *Tuorla Observatory, University of Turku, Väisäläntie 20, FIN-21500 Piikkiö, Finland; jupere@utu.fi, jarkot@utu.fi*

² *European Southern Observatory, Karl-Schwarzschild-Str. 2, D-85748 Garching bei München, Germany*

³ *Max-Planck-Institut für Astronomie, Königstuhl 17, D-69117 Heidelberg, Germany; prieto@mpia-hd.mpg.de*

Accepted date + Received date

ABSTRACT

We present sub-arcsec near-infrared 1.5 – 2.5 μm moderate resolution long-slit spectra of eight nearby Seyfert galaxies ($z < 0.01$), both parallel to the ionization cone and perpendicular to it. These spectra complement similar data on six Seyferts, presented in Reunanen, Kotilainen & Prieto (2002), and are used to study the spatial extent of the line emission, integrated masses of excited H_2 and the excitation mechanisms of interstellar gas.

Large concentrations of molecular gas (H_2) are present in the nucleus regardless of the Seyfert type. The spatial extent of the H_2 emission is larger perpendicular to the cone than parallel to it in 6/8 (75 %) galaxies, in agreement with the unified models of Active Galactic Nuclei. The FWHM sizes of the nuclear H_2 emission range from < 20 pc to ~ 300 pc, and are larger than the predicted sizes for molecular torus (1-100 pc). Thus the emission likely arises from the material surrounding the torus rather than directly from the torus.

Broad $\text{Br}\gamma$ was detected in nearly half of the optically classified Seyfert 2 galaxies, including two objects with no evidence for hidden polarized Broad Line Region. This high detection rate stresses the importance of extinction effects as the main cause for the Seyfert dichotomy.

$\text{Br}\gamma$ and $[\text{Fe II}]$ correlate both spatially and kinematically. Nuclear $[\text{Fe II}]$ emission is generally blueshifted which together with high $\text{Br}\gamma/[\text{Fe II}]$ ratios suggests shocks as the dominant excitation mechanism in Seyfert galaxies.

Bright coronal emission lines $[\text{Si VI}]$ and $[\text{Si VII}]$ are common in Seyferts, as they are detected in ~ 60 % of the galaxies. In three galaxies the coronal lines are extended only in the direction parallel to the cone. This could be explained by a strongly collimated radiation field or, most plausibly, by shock excitation due to the jet or superwind interacting with the interstellar medium.

Key words: galaxies:active – galaxies:nuclei – galaxies:Seyfert – infrared:galaxies

1 INTRODUCTION

In the currently favoured unified models of Active Galactic Nuclei (AGN; e.g. Antonucci 1993), a thick molecular torus surrounds the nucleus. In Seyfert 1 (Sy1) galaxies the nucleus and the Broad Line Region (BLR) are visible, while in Seyfert 2 (Sy2) galaxies the torus obscures the nucleus and the BLR and only the Narrow Line Region (NLR) is visible. Evidence for the unified models includes the detection of polarized broad lines in many Sy2s (e.g. Moran et al. 2000), believed to be light from the obscured BLR reflected into our line-of-sight, and cone-like $[\text{O III}]$ structures (e.g. Mulchaey,

Wilson & Tsvetanov 1996), almost invariably aligned with the radio jets.

The predicted size of the molecular torus in AGN ranges from 1 to 100 pc (e.g. Pier & Krolik 1993). Adequate spatial resolution to search for material associated with the torus, with a minimized contamination from circumnuclear star formation, can be achieved in the near-infrared (NIR; e.g. Veilleux, Goodrich & Hill 1997), where a wealth of emission and absorption lines are available. However, until recently such NIR spectroscopic studies have been made at only moderate spatial resolution (Veilleux et al. 1997: 3 arcsec aperture, $R = 1400$; Winge et al 2000: 7–8 arcsec, $R = 250$; Sosa-Brito et al. 2001: 2 arcsec, $R = 1100$), and/or with

only one slit position angle (PA) along the radio axis or the major axis of the [O III] emission (e.g. Storchi-Bergmann et al. 1999), and thus have not been able to derive the geometry of the molecular emission.

In Reunanen, Kotilainen & Prieto (2002; hereafter Paper I), we presented long-slit 1.5–2.5 μm moderate resolution spectroscopy of the first six galaxies in our sample of nearby ($0.0018 < z < 0.010$) Seyfert galaxies of both types with an ionization cone. In this paper, we complement these results with similar data on eight additional Seyferts, thus the size of the final sample is 14 Seyferts. These data are used to trace the spatial distribution, dynamics and excitation of molecular and nebular gas, and to determine the mass of hot ($T > 1000$ K) molecular gas in the central regions. In forthcoming publications, we shall study the stellar populations and star forming histories of the sample, in comparison with non-Seyfert spirals.

This paper is organized as follows: In Section 2 the observations, data reduction and methods used in the analysis are briefly summarized. In Section 3 the results for individual galaxies are discussed, and in Section 4 we present the conclusions based on the full sample of 14 galaxies. Throughout this paper, $H_0 = 75 \text{ km s}^{-1} \text{ Mpc}^{-1}$ and $q_0 = 0.5$ are assumed.

2 OBSERVATIONS, DATA REDUCTION AND METHODS OF ANALYSIS

The observations and data reduction are described in detail in Paper I. Here only a brief summary is given. Eight nearby Seyferts were observed in December 2000 with the 3.5 m ESO New Technology Telescope (NTT), using the 1024×1024 px SOFI camera (Lidman, Cuby & Vanzi 2000) with pixel scale $0.288 \text{ arcsec px}^{-1}$. The average seeing during the observations was $\sim 0.9 \text{ arcsec FWHM}$. The spectra were taken with the red grism with resolution $R = 980$ and slit width 1.0 arcsec . The wavelength range covered is 1.5–2.5 μm and the useful slit length $\sim 2 \text{ arcmin}$. Short broad-band *JHKs* images were also obtained, except for NGC 1068 and NGC 3783, for which we used the images from Peletier et al. (1999) and Mulchaey, Regan & Kundu (1997), respectively. The properties of the galaxies (redshift, scale, inclination, PA of the major axis, morphology, AGN type), the PAs of the slit, total integration time and the spatial resolution of the *K*-band spectra are given in Table 1.

The long-slit spectra were taken both parallel and perpendicular to the cone, in two positions along the slit separated by $\sim 2 \text{ arcmin}$. Data reduction using IRAF¹ included sky subtraction, flatfielding using dome flats, bad pixel and cosmic ray removal, and wavelength calibration from OH sky lines and Xe arc lamp. The spectra were averaged to remove residual continuum and OH sky lines, divided by an atmospheric standard star, and flux calibrated. All the spectra of a given galaxy were combined and the central 1.5 arcsec (5 px) spectrum was extracted, within an effective aperture of 1.4 arcsec diameter. The emission line fluxes and equivalent

widths in this aperture are given in Table 2. The quoted errors are generally dominated by the continuum fitting, and are 1σ except 3σ for upper limits. Because of telluric residuals, the uncertainties of 1–0 S(3) and [Si VI] are larger, 20–40 % of the flux. In order to trace the extended emission, 3 pixels were usually binned together. For the faintest emission, even larger binsizes were used.

Extinction was estimated by comparing the integrated colours from the spectra with the colours of normal, unobscured spiral galaxies ($H-K = 0.22$; Hunt et al. 1997). Although this continuum extinction may not be correct for the line emission, the difference is unlikely to be large, as discussed in Paper I. The effect of including the nuclear emission lines in the continuum colors is negligible, up to $A_K = 0.02$ in NGC 2992. We have assumed the extinction law $A_\lambda \propto \lambda^{-1.85}$ from Landini et al. (1984) and a foreground dust screen. The extinction for the central region is given in Table 2 and in the spatial profile figures.

Possible mechanisms for the H₂ emission in galaxies are thermal (collisional) excitation by shocks (e.g. Hollenbach & McKee 1989), UV radiation in dense clouds (e.g. Sternberg & Dalgarno 1989) or X-rays (e.g. Gredel & Dalgarno 1995), and UV pumping (fluorescence; e.g. Black & van Dishoeck 1987). The emission line ratios can be used to distinguish between these excitation mechanisms. For example, the H₂ line ratio 2–1 S(1)/1–0 S(1) is lower for thermal excitation than for UV fluorescence, while [Fe II]/Br γ is higher in X-ray or shock excited regions than in H II regions (e.g. Colina 1993). X-ray excitation can also produce lower [Fe II]/Br γ ratios, but this would lead to extreme 1–0 S(1)/Br $\gamma > 100$. The H₂ line ratios 2–1 S(1)/1–0 S(1) and 1–0 S(0)/1–0 S(2) can be used to derive the vibrational excitation temperature T_{vib} and the rotational temperature T_{rot} , respectively.

The mass of the excited molecular hydrogen in the nucleus was derived using the transition probabilities by Wolniewicz, Simbotin & Dalgarno (1998), the vibration temperature and thermal equilibrium, and are given in Table 4. If T_{vib} is unknown, it is assumed to be 2000 K. This leads to a factor of ~ 2 uncertainty in the mass, if the real temperature is > 1500 K. Below 1500 K the fraction of H₂ in the $v = 1, J = 3$ energy level declines rapidly and the mass is underestimated by a factor of ~ 10 if $T = 1000$ K. However, 1–0 S(1) emission is likely to be biased towards warmer gas, because the $E_{\text{upper}} = 6950$ K for the $v = 1, J = 3$ level. We have also determined the average surface density of the excited H₂ in the nucleus.

The Gaussian FWHM sizes for H₂ and [Fe II] in Table 4 have been obtained by measuring the line flux in each column across the nuclear region and are corrected for the seeing. The number of columns fitted was chosen to include the nuclear knot and exclude any additional extended emission. The structures probed here correspond to physical scales of 100–200 pc, depending on the distance of the galaxies.

3 RESULTS

The nuclear $30 \times 30 \text{ arcsec}$ *K*-band images of the galaxies, with the slit positions overlaid, are shown in Fig. 1 and the *H*- and *K*-band nuclear spectra in Fig. 2. The spatial extent of the main emission lines is shown in Figs. 3 and 10, velocity fields of the main emission lines in Fig. 5, and the spectra at

¹ IRAF is distributed by the National Optical Astronomy Observatories, which are operated by the Association of Universities for Research in Astronomy, Inc., under cooperative agreement with the National Science Foundation

Table 1. Observational properties of the galaxies.

Galaxy	z	Scale pc/''	i °	PA °	Morphology	Type	PA _∥ °	PA _⊥ °	t_{int} min	Resolution ''
this work:										
NGC 1068	0.00379	75	32	70	(R)SA(rs)b	Sy2	12	-78	32,32	0''9
NGC 1365	0.00546	108	57	32	(R')SB(s)b	Sy1.8	-55	35	48,48	0''7
NGC 2110	0.00779	154	42	157	SAB0 ⁻	Sy2	-3	87	48,48	0''9
ESO 428-G14	0.00544	108	53	135	SA:(l)0 ⁺	Sy2	-50	40	32,32	0''8
NGC 2992	0.00771	152	72	22	Sa pec	Sy2	-60	30	64,56	0''8
NGC 3081	0.00795	157	39	158	(R ₁)SAB(r)0/a	Sy2	-20	70	32,32	1''0
NGC 3783	0.00973	192	27	160	(R')SB(r)a	Sy1	75	-15	48,40	0''9
NGC 7582	0.00540	107	65	157	(R' ₁)SB(s)ab	Sy2	64	-26	56,40	0''8
Paper I:										
NGC 1097	0.00425	82	46	141	(R' ₁)SB(r'l)b	Sy1	15,54	-36,-75	2×32,2×48	1''0
NGC 1386	0.00289	56	74	25	SB(s)0 ⁺	Sy2	1	-89	48,64	1''1
NGC 1566	0.00483	94	28	30	(R' ₁)SAB(rs)bc	Sy1	-42	48	48,64	1''0
NGC 3227	0.00382	74	56	158	SAB(s) pec	Sy1.5	15	-75	48,80	1''0
NGC 4945	0.00194	19	78	43	SB(s)cd: sp	Sy2	-64	26	32,64	0''9
NGC 5128	0.00179	19	65	30	S0 pec	Sy2	50	-40	16,48	0''9

Table 2. Observed emission line fluxes within the nuclear 1.4 arcsec diameter aperture, after adding all the data from different slit PAs. The fluxes (*first row*) are in units of 10^{-15} erg cm⁻² and the Gaussian FWHMs (*second row*) in Å. The width of the lines has not been corrected for instrumental profile (30–32 Å depending on wavelength). Decomposition into two components: (a) 28±4 (5% of the total flux) and 163±6 Å, (b) 33±3 (10%) and 178±20 Å, (c) 42.6±4 (6%) and 185±6 Å, (d) 47±10 (7%) and 222±7 Å, (e) 33.9±1.1 (9%) and 205±5 Å

Line Nucleus	λ μm	NGC1068 Sy2	NGC1365 Sy1.8	NGC2110 Sy2	ESO428-G14 Sy2	NGC2992 Sy2	NGC3081 Sy2	NGC3783 Sy1	NGC7582 Sy2
A _K		2.49	1.14	0.85	0.29	0.95	0.28	1.25	1.51
[FeII]	1.644	29.1±3.2 49.8±4.5	4.1±0.4 46.5±8.2	23.4±0.2 42.1±0.3	7.9±0.1 37.1±0.4	11.8±0.3 36.8±0.5	0.5±0.1 25.5±2.7	2.6±0.3 33.5±3.4	7.1±0.4 30.2±2.0
1-0 S(3)	1.958	6.2 36.0	3.1 33.7	6.5 30.0	3.2 43.1	2.2 37.4	...
[SiVI]	1.964	299 84.3	9.4 49.3	7.8 41.0	8.1 36.1	7.7 42.0	9.8 58
1-0 S(2)	2.034	<7	<0.8	2.4 ±0.3 44.1±4.8	1.1±0.1 38.6±1.7	1.9±0.1 32.2±1.8	0.9±0.1 37.4±2.2	<0.4	2.0±0.4 35.6±8.0
[AlIX]	2.043	<7	<1.0	<0.3	<0.2	1.2±0.2 33.8±4.6	0.5±0.1 33.1±4.8	<1.6	<0.8
HeI	2.058	<7	6.0±0.9 68±13	<0.3	1.0±0.1 35.2±2.6	8.4±0.7 <i>a</i>	0.4±0.1 29.7±5.1	7.9±1.5 255±33	<0.7
1-0 S(1)	2.122	13.2±4.0 36.9±8.5	<0.8	4.4±0.3 40.4±1.3	3.1±0.2 40.3±1.1	6.5±0.1 33.6±0.4	1.6±0.1 33.8±1.2	1.1±0.3 37.8±9.6	3.8±0.5 45.4±3.9
Br γ	2.166	34.6±4.1 74.3±8.9	23.2±0.8 90.3±3.5	4.8±0.7 <i>b</i>	3.7±0.1 44.6±0.7	23.7±0.5 <i>c</i>	1.0±0.1 29.3±1.8	25.5±1.2 <i>d</i>	34.9±1.2 <i>e</i>
1-0 S(0)	2.224	<9	<0.8	1.5±0.3 42.1±9.7	0.7±0.1 26.1±2.9	1.5±0.2 33.0±2.6	<0.3	<0.4	<0.7
2-1 S(1)	2.248	<8	<0.9	1.2±0.2 53.7±6.1	0.5±0.1 39.6±3.3	1.2±0.2 31.6±3.4	<0.2	<0.4	<0.8
[CaVIII]	2.321	67±9 87±12	<1.3	<0.5	< 0.45	<1.5	1.2±0.2 57.3±8.4	23.9±0.6 38.3±7.7	<1.1
1-0 Q(1)	2.407	<22	<1.5	3.3±0.4 39.6±4.4	<0.8	3.6±0.2 28.2±1.4	0.7±0.2 19.9±4.7	<0.8	<1.5
1-0 Q(3)	2.424	<37	<1.8	<1.4	1.4±0.4 26.4±7.2	<0.3	1.4±0.1 35.1±2.1	<1.1	<1.9
[SiVII]	2.483	467±75 112±18	<3.3	<4.2	6.6±1 36.3±2.9	16±5 110±30	7.6±0.8 48.2±3.9	15.3±3.1 44±10	21.6±5.4 47.8±9.8

Table 3. Dereddened emission line ratios relative to Br γ . The galaxies from Paper I are included to facilitate comparison. For NGC 1386 a 0.6 arcsec slit was used.

Nucleus	1068 Sy2	1097 Sy1	1365 Sy1.8	1386 Sy2	1566 Sy1	2110 Sy2	E428 Sy2	2992 Sy2	3081 Sy2	3227 Sy1.5	3783 Sy1	4945 Sy2	5128 Sy2	7582 Sy2
[Fe II]	4.0	>2.2	0.36	6.84	0.48	8.34	2.55	0.93	0.64	1.47	0.22	3.77	14.6	0.53
[Si VI]	13.8	6.03	2.66	0.39	8.73	0.36	0.42	0.37
1-0 S(2)	<0.3	>4.3	<0.04	0.81	0.05	0.56	0.23	0.09	0.91	0.24	<0.02	1.49	<0.2	0.11
He I	<0.3	...	0.41	<0.2	<0.04	<0.07	0.28	0.39	0.37	<0.02	0.35	0.35	<0.2	<0.03
1-0 S(1)	0.42	>4.4	<0.04	1.14	0.28	0.93	0.84	0.28	1.60	0.54	0.21	3.10	2.03	0.07
1-0 S(0)	<0.3	>1.4	<0.04	<0.2	<0.04	0.30	0.18	0.06	0.21	0.15	<0.02	0.53	0.34	<0.02
2-1 S(1)	<0.2	...	<0.04	<0.2	<0.04	0.24	<0.2	0.05	<0.2	0.04	<0.02	0.35	<0.2	<0.03
[Ca VIII]	1.46	...	<0.05	2.09	<0.06	<0.1	<0.2	<0.06	1.66	<0.01	0.08	<0.1	<0.2	<0.03
[Si VII]	7.96	...	<0.12	9.58	<0.3	<0.8	1.7	<2.0	7.33	0.24	0.46	<0.2	<0.3	0.45

different distances from the nucleus in Figs. 4, 8 and 9. The nuclear-subtracted spectra have been obtained by matching the flux of the K -band CO lines in the off-nuclear (0.7-1.6 arcsec radius from the nucleus) spectra to the 1.4 arcsec diameter nuclear aperture and subtracting the result from the nuclear spectra. The nuclear-subtracted spectra are included here to better show the weak nuclear emission lines. The subtracted spectra are not shown for NGC 1068, NGC 1365 or NGC 3783 because these galaxies have very weak CO lines (CO index ~ 0).

3.1 NGC 1068

NGC 1068 is a nearby ($z = 0.00379$; distance = 15.1 Mpc) (R)SA(rs)b galaxy. It has an extensively studied Sy2 nucleus with high extinction derived towards the BLR ($A_V > 50$ mag), as evidenced by the non-detection of broad Br α 4.05 μm (Lutz et al. 2002). NGC 1068 also harbors a star forming ring with diameter ~ 15 arcsec (~ 1.1 kpc; e.g. Davies, Sugai & Ward 1998). Rouan et al. (1998) found K -band extended emission along PA = 102° , up to 15 pc radius, interpreted as the equatorial plane of an inclined torus. This extension can also be seen in the LM -bands (Marco & Alloin 2000). NGC 1068 has an [O III] cone, which extends to ~ 7.5 arcsec at PA = 35° (Evans et al. 1991).

The H - and K -band nuclear spectrum of NGC 1068 (Fig. 2) resembles that of NGC 5128 (Paper I), having an almost power-law like continuum shape. The most prominent features in the nuclear spectra are the coronal lines [Si VI] 1.964 μm , [Ca VIII] 2.321 μm and [Si VII] 2.483 μm . The other emission lines detected in the nucleus are [Fe II] 1.644 μm , H $_2$ 1-0 S(1) 2.122 μm and Br γ 2.166 μm . Also Pa α 1.876 μm is prominent, but its usefulness is limited by telluric residuals. Nuclear H $_2$ emission is faint.

1-0 S(1) is the most extended line and is detected up to 5-7 arcsec (300 pc) from the nucleus parallel to the cone and ~ 4 arcsec perpendicular to it. [Fe II] and Br γ are extended ~ 4 arcsec from the nucleus. Br γ , [Fe II], H $_2$ and He I 2.058 μm are furthermore detected in the star forming ring ~ 15 arcsec (~ 1.1 kpc) from the nucleus. [Si VI] 1.964 μm is the strongest emission line in the nucleus, [Fe II] between the nucleus and the ring, and Br γ in the ring. However, generally the equivalent widths of the emission lines in the ring are smaller than e.g. in the rings of NGC 1097 (Paper I; Kotilainen et al. 2000) or NGC 1365 (see below).

The kinematics of NGC 1068 has been discussed in de-

tail by Schinnerer et al. (2000) based on CO millimeter lines and by Alloin et al. (2001), based on H $_2$ emission. The velocity curve of [Fe II] parallel to the cone is much steeper within the inner 3 arcsec (230 pc) than that of H $_2$. At larger radii, [Fe II] seems to follow H $_2$ more closely. Furthermore, within the steep part of the velocity curve, the kinematics of the [Fe II] depends only on the position along the slit. Thus it seems very likely that [Fe II] is excited by the outflowing material in the jet. In addition, parallel to the cone [Fe II] has two velocity components and thus the line profile changes within the few inner arcsec (Fig. 6). Similar structure is also visible in the Br γ and coronal lines.

The nuclear [Fe II]/Br γ ratio = 4 (Table 3) is higher than star formation models predict (e.g. Colina 1993). The 1-0 S S(1)/Br γ ratio = 0.4 is in agreement with the star formation origin for H $_2$ as a result of UV heating from OB stars (Puxley et al. 1990). Whether the heating mechanism is thermal or fluorescence is not clear, because no 2-1 S(1) or 1-0 S(0) emission was detected in the nucleus.

The derived parameters, including the density and mass of the molecular hydrogen both in the nuclear 1.4 arcsec aperture and integrated within the starforming ring as traced by Br γ , and the spatial extent of different lines are given in Table 4. In the nuclear 1.4 arcsec aperture, the column density of the excited molecular hydrogen is 1.3×10^{19} cm $^{-2}$ (corresponding to $M_{\text{H}_2} = 1800 M_\odot$), assuming $T = 2000$ K. The FWHM size of the nuclear H $_2$ emission cannot be measured reliably as the emission is weak with respect to the continuum.

Several IR coronal lines have previously been detected in NGC 1068 (e.g. Oliva & Moorwood 1990). All the detected coronal lines ([Si VI] 1.964 μm , [Ca VIII] 2.321 μm and [Si VII] 2.483 μm) are resolved parallel to the cone (Fig. 6), and are more extended toward north (~ 2 arcsec) than south, in agreement with the NICMOS image of [Si VI] emission by Thompson et al. (2001). The velocity curves of the coronal lines resemble the weaker of the two [Fe II] velocity components. Extended coronal line emission can in principle only be excited by shocks in the interstellar medium that are produced either by a jet or AGN-generated winds.

3.2 NGC 1365

NGC 1365 is a nearby ($z = 0.00546$; distance = 21.7 Mpc) SB(s)b galaxy in the Fornax cluster with a Seyfert 1.8 nucleus. NGC 1365 is undergoing intense starburst activity in

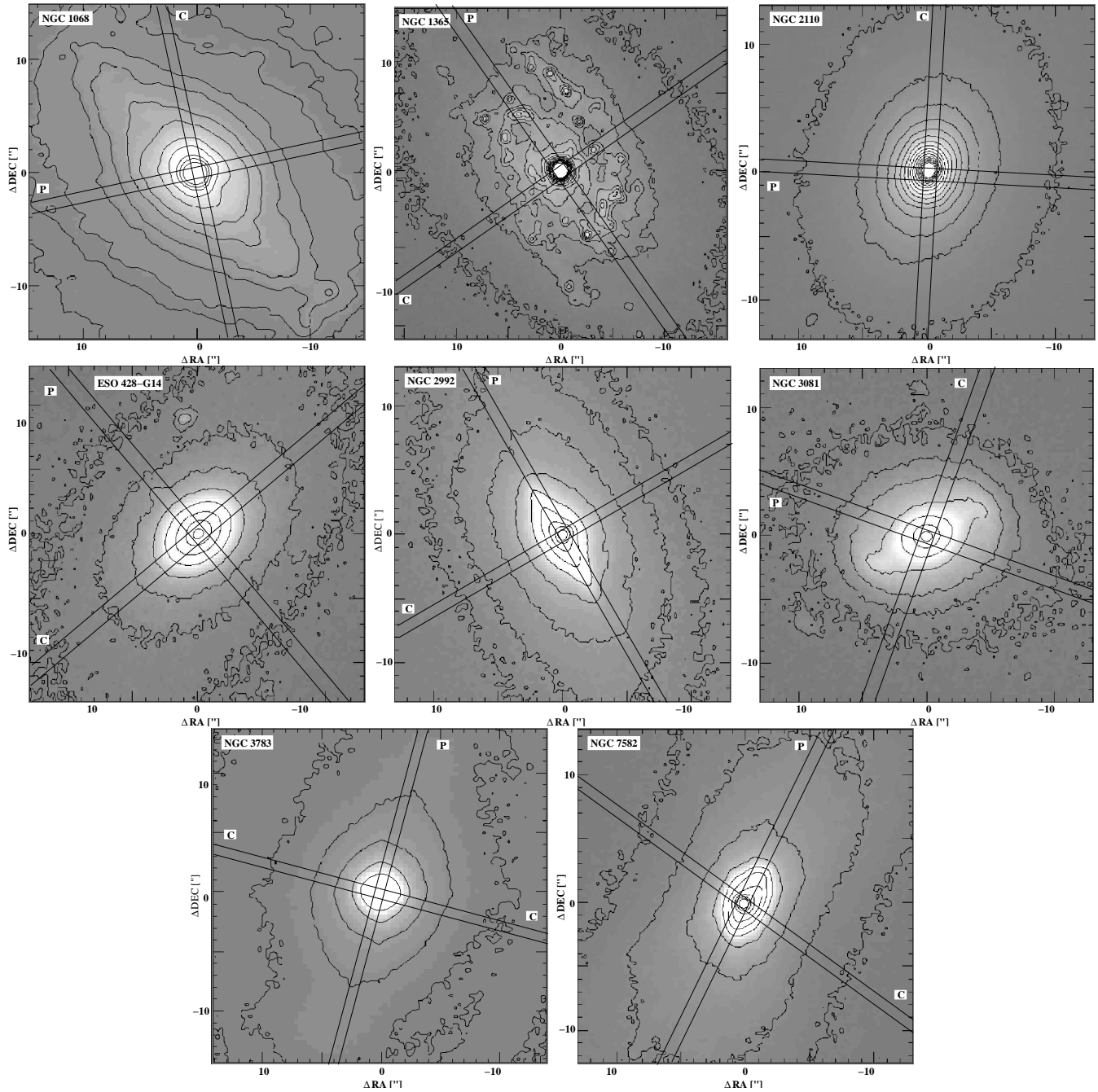


Figure 1. The near-infrared images of NGC 1068 (*top left*; *H*-band from Peletier et al. 1999), NGC 1365 (*top center*), NGC 2110 (*top right*), ESO 428-G14 (*middle left*), NGC 2992 (*middle center*), NGC 3081 (*middle right*), NGC 3783 (*bottom left*; *K*-band from Mulchaey et al. (1997)) and NGC 7582 (*bottom right*). All images are in the *K*s-band except as marked. North is up and East to the left. Slit positions are indicated in the images, marked with C for parallel to the cone, on the side where the cone is stronger, and P perpendicular to the cone.

its bar concentrated into a ring-like structure with a diameter of ~ 15 arcsec (1.6 kpc) (e.g. Kristen et al. 1997; Stevens et al. 1999). The hollow high-excitation outflow cone of NGC 1365 ($PA = 130^\circ$; e.g. Kristen et al. 1997) is parallel to the radio jet (Sandqvist et al. 1995).

The *H*- and *K*-band nuclear spectra of NGC 1365 are shown in Fig. 2, the extent of the main emission lines in Fig. 3 and the spectra at different distances from the nucleus in Fig. 4. The most intriguing feature in the spectra is that

unlike all the other galaxies in our sample, NGC 1365 does not exhibit nuclear H_2 emission. This may be partly due to the strong non-stellar continuum which dominates the *K*-band emission. In fact, only He I $2.058 \mu\text{m}$, several Brackett series lines, and weak [Fe II] $1.64 \mu\text{m}$, are detected. $Br\gamma$ is broad with a FWHM of $\sim 1190 \text{ km s}^{-1}$, and no evidence for the narrow component is seen (Fig. 7).

$Br\gamma 2.166 \mu\text{m}$ is the only extended nuclear emission line. It decays smoothly towards the star forming regions

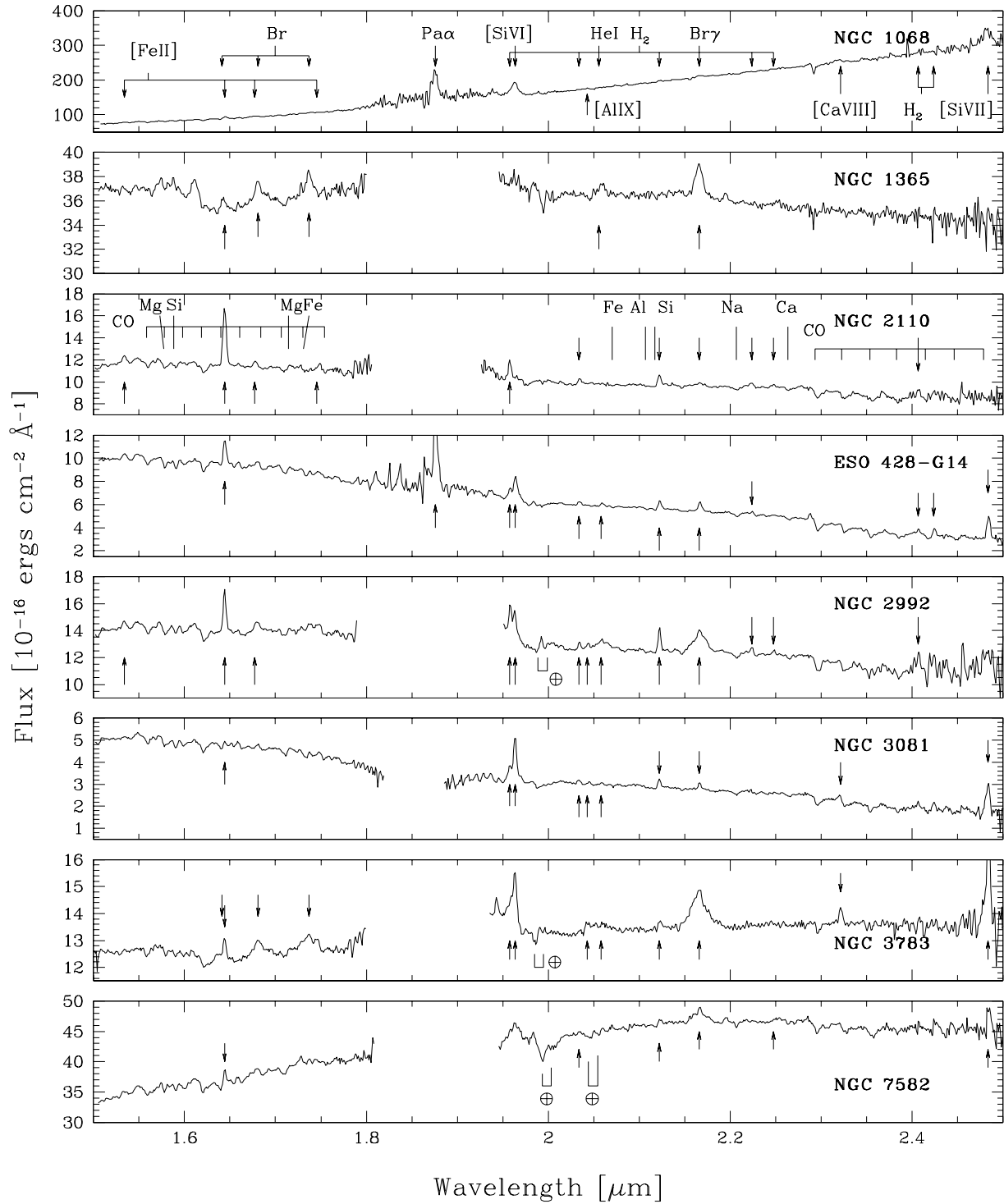


Figure 2. The nuclear H - and K -band spectra in a nuclear 1.4 arcsec aperture for, from top to bottom, NGC 1068, NGC 1365, NGC 2110, ESO 428-G14, NGC 2992, NGC 3081, NGC 3783 and NGC 7582. All the detected emission lines have been labelled in the first panel, and marked with arrows in the subsequent panels. The main absorption lines have been marked in the panel of NGC 2110. Atmospheric features are marked with \oplus .

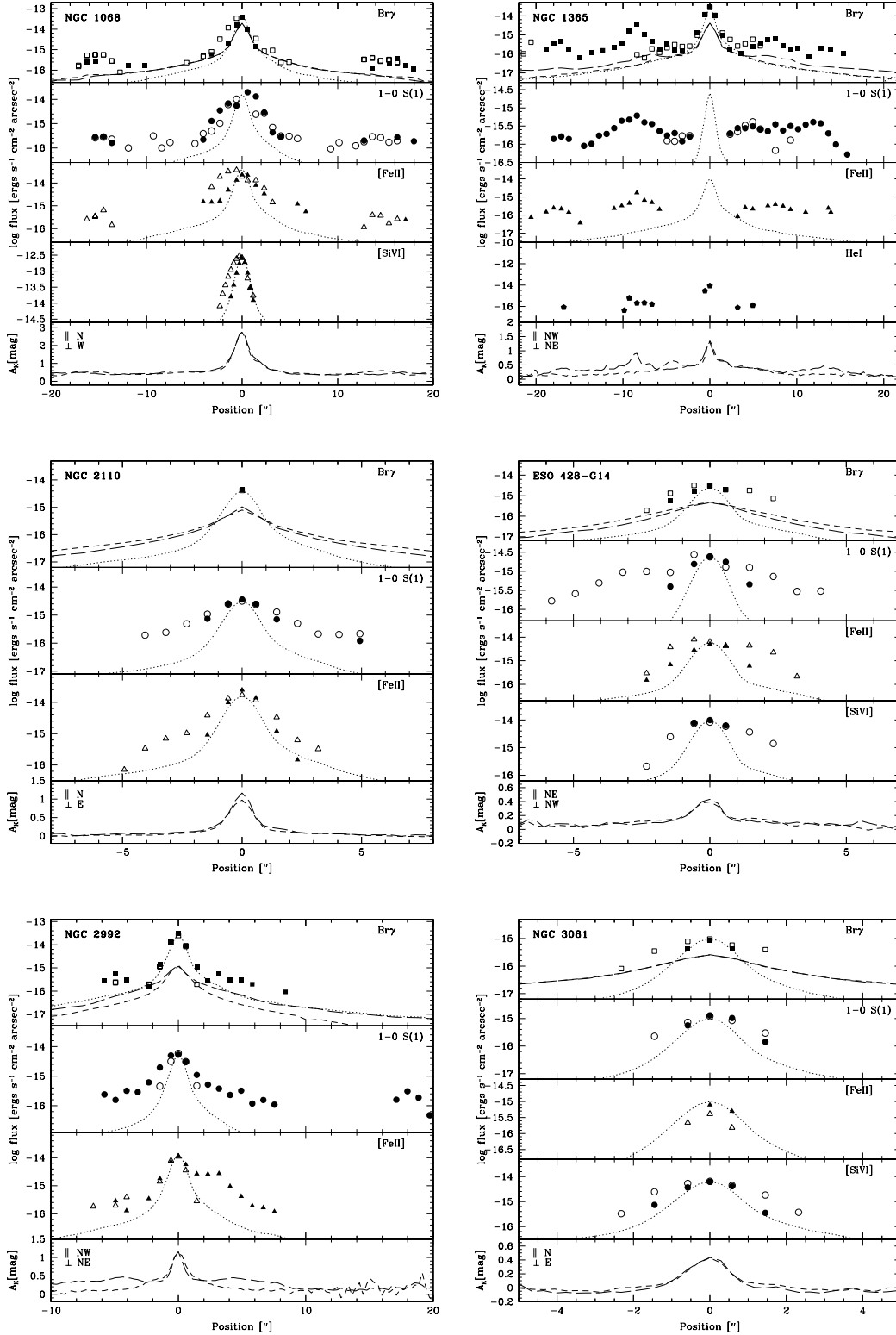


Figure 3. The observed line emission in NGC 1068 (upper left), NGC 1365 (upper right), NGC 2110 (middle left), ESO 428-G14 (middle right), NGC 2992 (lower left) and NGC 3081 (lower right). Open symbols indicate parallel to the cone and filled symbols perpendicular to the cone. The PSF is indicated by dotted lines. Extinction is plotted in the lowermost panel of each sub-figure. Negative direction along the slit has been marked. In the uppermost panel, the $2.1 \mu\text{m}$ continuum emission is indicated parallel to the cone (short-dashed line) and perpendicular to it (long-dashed line). In most cases three columns have been binned together to lower noise.

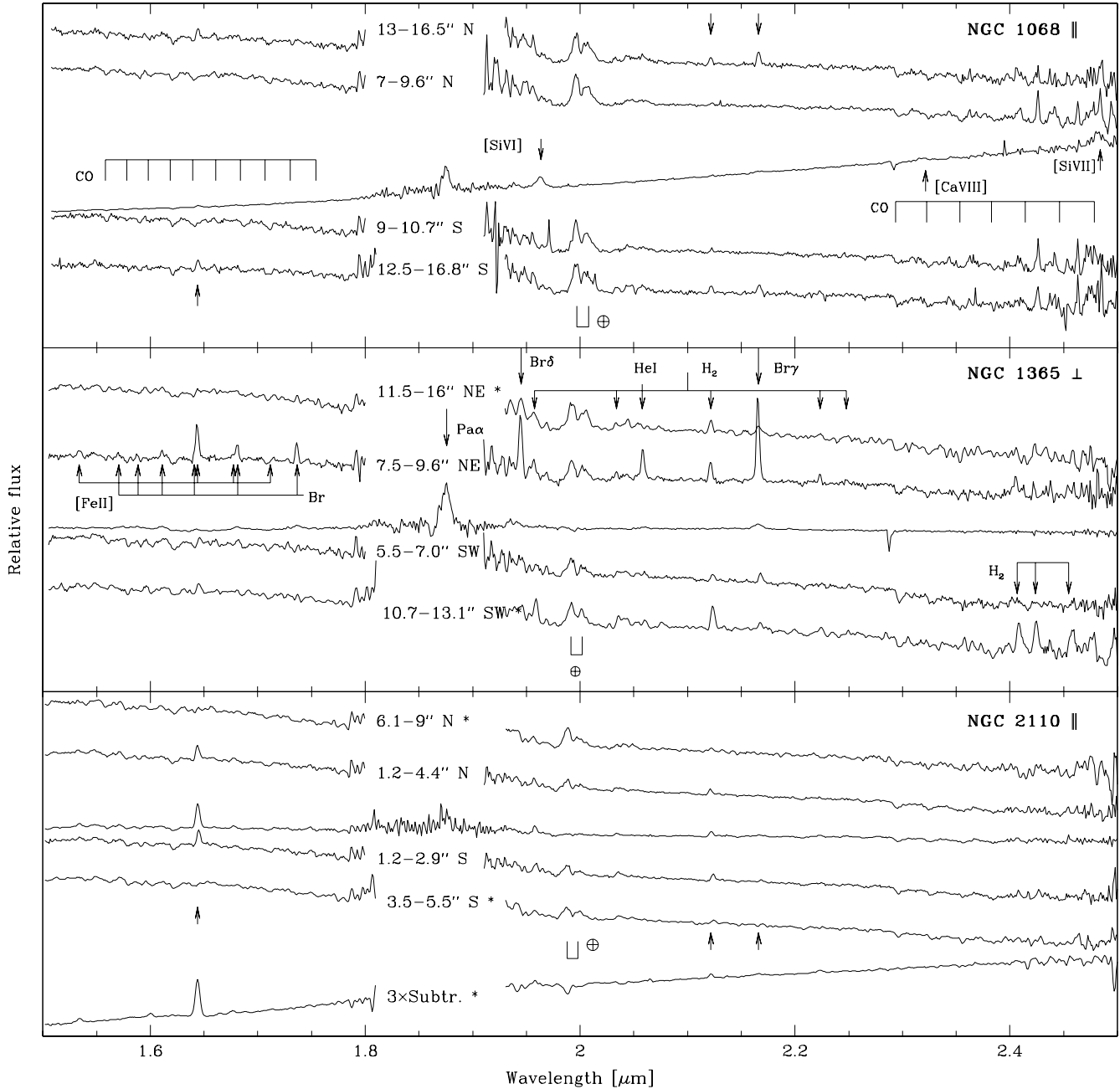


Figure 4. The 1.5–2.5 μm spectra of, from top to bottom, NGC 1068, NGC 1365 and NGC 2110, at different positions along the slit. The K-band flux was scaled to match the flux in the nuclear 1.4 arcsec aperture, and the spectra were placed at uniform intervals to facilitate comparison between different regions. The absorption features at 2.0 μm and 2.05 μm are due to imperfect atmospheric cancellation. The nuclear subtracted spectrum was obtained as discussed in the text. The spectra marked with a star have been smoothed with three pixel boxcar function. The direction with respect to the cone has been marked next to the label on the upper right corner in each panel.

(~ 6 arcsec; 600 pc), where other emission lines (e.g. H_2 and HeI) become visible. [Fe II] is detected perpendicular to the ionization cone, but not parallel to it, as there are no strong star forming regions coincident with the slit in that direction. There is a fair correlation between 1–0 S(1), Br γ , [Fe II] and HeI in the star forming ring, suggesting a common origin. This is further supported by the fairly similar velocity curves in the ring (Fig. 5).

The velocity field of NGC 1365 is shown in Fig. 5. The

nuclear Br γ emission is blueshifted by ~ 220 km s^{-1} with respect to the overall velocity curve. This blueshift is also observed in the H -band Brackett lines, which are also broad (~ 1170 km s^{-1}).

No H_2 lines are detected in the nucleus. The 3σ upper limit for 1–0 S(1) emission in the nuclear 1.4 arcsec aperture is 8×10^{-16} $\text{ergs cm}^{-2} \text{s}^{-1}$ giving an upper limit in an 1.4 arcsec aperture of $60 M_{\odot}$. The integrated mass of the

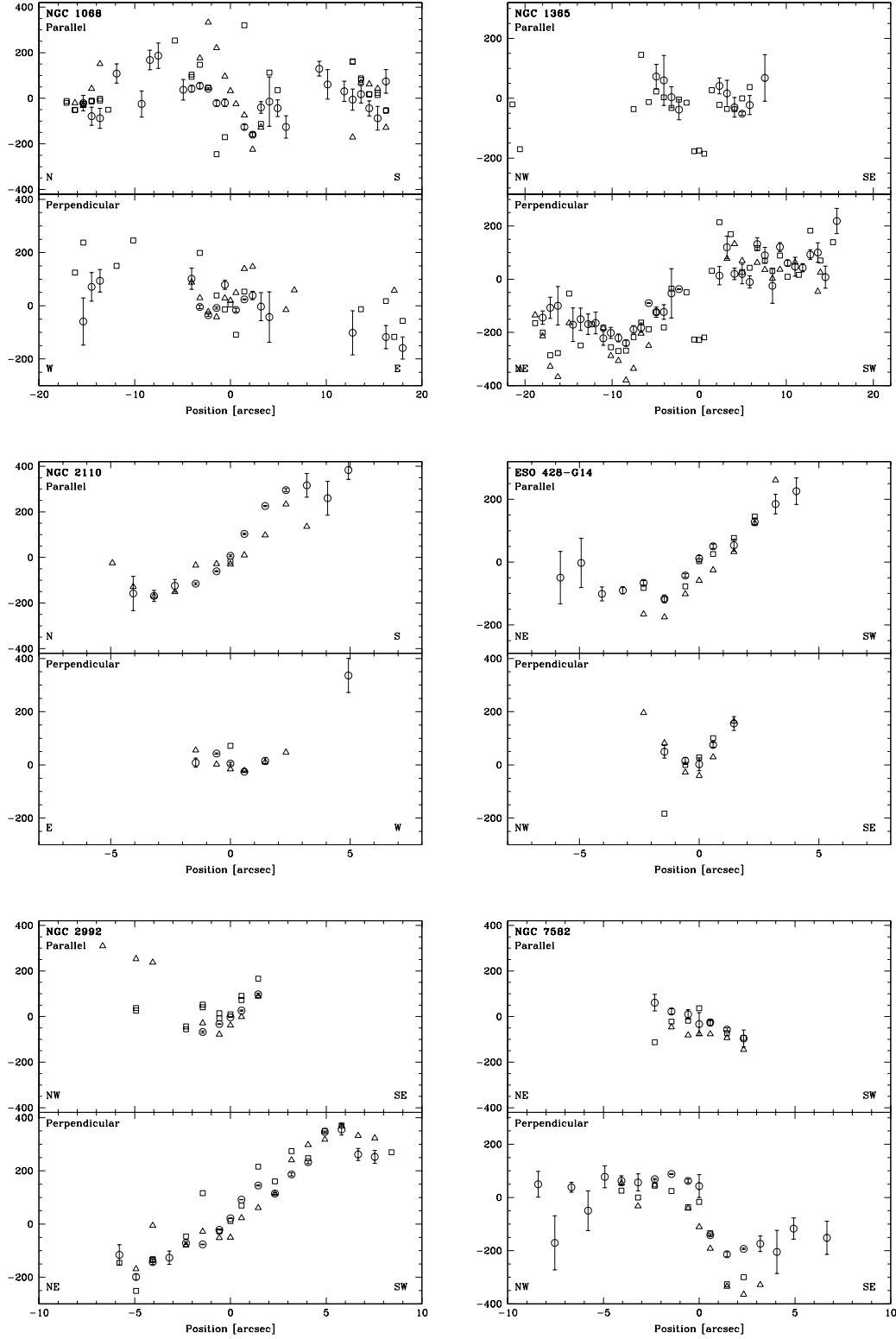


Figure 5. The observed velocity field in units of km s^{-1} in the 1-0 S(1) (circles with error bars), $\text{Br}\gamma$ (squares) and [Fe II] (triangles) lines for NGC 1068 (upper left), NGC 1365 (upper right), NGC 2110 (middle left), ESO 428-G14 (middle right), NGC 2992 (bottom left) and NGC 7582 (bottom right). The x-axis shows the position along the slit.

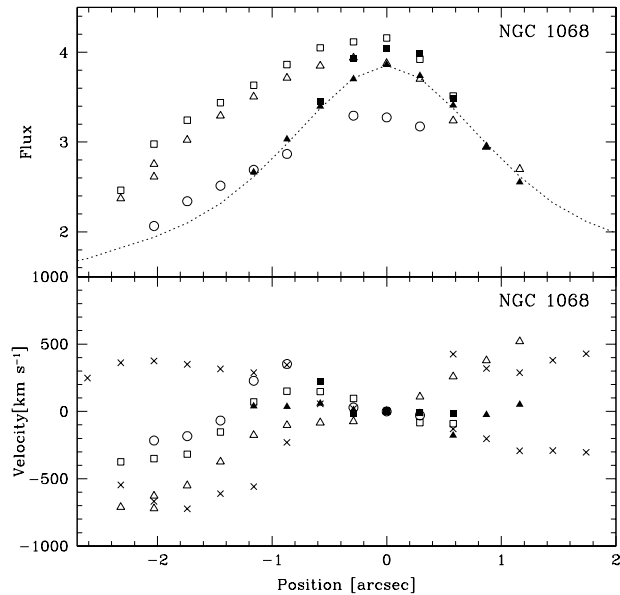


Figure 6. The spatial extent (*upper panel*) and velocity field (*lower panel*) of the coronal [Si VI] 1.964 μm (triangles), [Ca VIII] 2.321 μm (circles) and [Si VII] 2.483 μm line emission (squares) in NGC 1068. Open symbols denote parallel to the cone and filled symbols perpendicular to it. PSF is indicated with a dotted line. The two velocity components of [Fe II] 1.644 μm are indicated with crosses.

excited hydrogen is 290 M_{\odot} perpendicular to the cone and ~ 90 parallel to it.

Perpendicular to the ionization cone, there are three separate Br γ emission regions, the two innermost of which are associated with the starburst ring. These regions are also visible in the *H*-band Brackett lines, He I and [Fe II], which trace star formation, and also in 1–0 S(1). The equivalent width of Br γ reaches up to 70 \AA , much larger than e.g. in the ring of NGC 1097 (Kotilainen et al. 2000; ~ 15 \AA), implying recent star formation. Parallel to the cone there are no separate Br γ knots, but the ring shows off as a plateau in the spatial line emission profile. The extinction derived from the Br 10–4/Br γ and Br 11–4/Br γ -ratios ($A_K = 0.67$ and 0.69, respectively) is identical to that based on the continuum colour ($A_K = 0.68$). Notwithstanding the existence of a strong UV radiation field as evidenced by the Brackett lines, H $_2$ appears to be thermally excited, as the 2–1 S(1)/1–0 S(1) ratio is 0.16 ± 0.05 ($T_{\text{vib}} = 2600 \pm 400$ K).

3.3 NGC 2110

NGC 2110 is a nearby ($z = 0.00779$; distance = 31.0 Mpc) SAB 0 galaxy with a Sy2 nucleus. HST [O III] imaging shows a narrow 1 arcsec long jet-like feature (cone) at PA = 340° , and a weaker feature at PA = 160° (Mulchaey et al. 1994). The hard X-ray emission of NGC 2110 (Malaguti et al. 1999) is highly absorbed and indicates an obscured Sy1 nucleus. Storchi-Bergmann et al. (1999) found extended H $_2$ 1–0 S(1) emission, probably excited by central X-rays.

The nuclear *H*- and *K*-band spectrum of NGC 2110 (Fig. 4) is different from the more powerful Sy2s such as

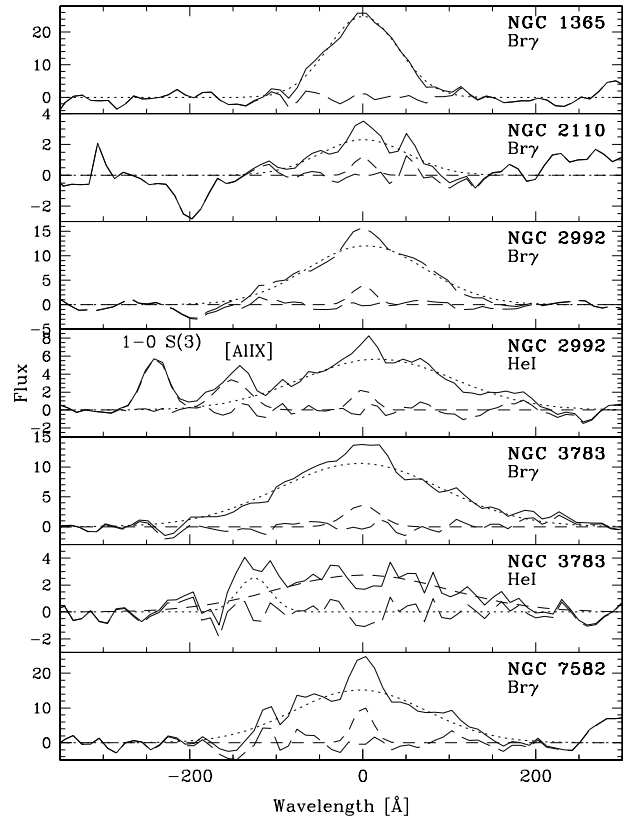


Figure 7. Decomposition of emission lines into narrow (*short dashed line*) and broad (*dotted line*) components and the residual (*long dashed line*) of the fit for NGC 1365, NGC 2110, NGC 2992, NGC 3783 and NGC 7582. The continuum has been subtracted with a second order polynomial.

NGC 1068 (this paper) and NGC 5128 (Paper I), appearing to have more contribution from the stellar continuum. [Fe II] 1.644 μm is by far the strongest line in the nucleus, where other detected lines are various H $_2$ lines and Br γ 2.166 μm . Br γ is rather weak, but has a faint broad component (FWHM ~ 2000 km s $^{-1}$; Fig. 7). No coronal lines are detected.

NGC 2110 has been previously observed spectroscopically in the NIR by e.g. Storchi-Bergmann et al. (1999). The presence of a broad component to the recombination lines has been under debate as Veilleux et al. (1997) found some evidence in Pa β 1.282 μm , but Storchi-Bergmann et al. (1999) did not detect this. We found the FWHM of Br γ to be ~ 1550 km s $^{-1}$, in fair agreement with Veilleux et al. (1200 km s $^{-1}$).

1–0 S(1) is the most extended line, followed by [Fe II], but even 1–0 S(1) can only be traced up to 4–5 arcsec (~ 700 pc) distance from the nucleus parallel to the cone and 1.5 arcsec (~ 300 pc) perpendicular to it with no separate emission regions. Surprisingly, Br γ is not extended, which excludes star formation as the origin of the extended [Fe II] emission. The total (nuclear) extent of [Fe II] emission is ~ 4 arcsec (0.6 kpc) parallel to the cone, and ~ 2 arcsec (300 pc) perpendicular to it. [Fe II] is spatially resolved in the nucleus and is more extended parallel to the cone.

The velocity curve of [Fe II] parallel to the cone is flat-

ter than that of H₂ close to the nucleus, in agreement with previous determinations (e.g. Knop et al. 2001). Further out the velocity curves of H₂ and [Fe II] are in better agreement. Perpendicular to the cone the curves are flatter than parallel to the cone.

The dereddened [Fe II]/Br γ ratio is ~ 8 , one of the highest in our sample, and [Fe II]/Br γ_{narrows} = 80. Thus, considering the different morphologies of [Fe II] and Br γ , [Fe II] is likely to be X-ray excited. Furthermore, there is a fair correlation between *Chandra* soft X-ray images (Weaver 2001) and the [Fe II] emission: the X-ray emission in NGC 2110 is more extended parallel to the cone than perpendicular to it, and more extended towards north than south. X-ray excitation (Maloney, Hollenbach & Tielens 1996) can also explain the H₂ emission in the nucleus, assuming that almost all of the gas is dense ($n = 10^5 \text{ cm}^{-3}$) and that there is a high ratio of the local X-ray energy deposition rate per particle to the gas density. Outside of the nucleus, H₂ may also be X-ray excited as 1–0 S(1)/[Fe II] ratio produced in X-ray excited gas depends strongly on the density of the gas and the intensity of the radiation, but this does not seem likely as the velocity fields of [Fe II] and H₂ are quite different.

Assuming $T_{\text{vib}} = 2000 \text{ K}$, we derive $N_{\text{H}_2} = 4.3 \times 10^{17} \text{ cm}^{-2}$ (corresponding to $M_{\text{H}_2} \simeq 250 M_{\odot}$) within the nuclear aperture. The total integrated M_{H_2} is larger parallel to the cone than perpendicular to it (220 vs. 190 M_{\odot}) and the FWHM of nuclear H₂ emission is larger parallel to the cone than perpendicular to it (320 pc vs. 230 pc).

3.4 ESO 428-G14

ESO 428-G14 is a nearby ($z = 0.00544$; distance = 21.6 Mpc) SA:(l)0⁺ galaxy with a Sy2 nucleus (Bergvall, Johansson & Olofsson 1986). It has a bent radio jet (Ulvestad & Wilson 1989), and an [O III] cone along the jet (Wilson & Baldwin 1989). The NLR of ESO 428-G14 consists of many thin strands closely related to the two-sided jet (Falcke et al. 1996).

The *H*- and *K*-band spectra of ESO 428-G14 are shown in Fig. 2 and Fig. 8. The strongest nuclear line is [Fe II] 1.644 μm , followed by Br γ 2.166 μm , various H₂ lines, and He I 2.058 μm . Two coronal lines [Si VI] 1.964 μm and [Si VII] 2.483 μm were also detected.

The nuclear H₂, [Fe II] and Br γ emission lines are all spatially resolved. 1–0 S(1) is the most extended line, extending up to ~ 7 arcsec (0.7 kpc) parallel to the cone, but only up to ~ 2 arcsec (210 pc) perpendicular to it. Also, both Br γ and [Fe II] are more extended parallel to the cone (up to ~ 3 arcsec; 320 pc) than perpendicular to it (~ 2 arcsec; ~ 200 pc). The morphologies of H₂, Br γ and [Fe II] are all similar parallel to the cone: the central peak is displaced 0.5 arcsec to NE and a separate peak is detected ~ 1.3 arcsec SW of the continuum nucleus. Br γ is narrow with no detectable broad component.

The velocity field of ESO 428-G14 is shown in Fig. 5. [Fe II] is blueshifted by $\sim 70 \text{ km s}^{-1}$ across the nuclear region. H₂ and Br γ appear to have similar dynamics, but in the NE peak Br γ is also blueshifted with respect to H₂. Thus it seems that the extended H₂ and Br γ emission share a same origin, probably in the star forming clouds.

The nuclear [Fe II]/Br γ ratio = 2.6 is higher than models suggest for star forming regions. The ratio is nearly con-

stant parallel to the cone up to ~ 2 arcsec from the nucleus. Perpendicular to the cone, the ratio is lower (~ 1.2) toward northwest. The 1–0 S(1)/Br γ ratio is also fairly constant, 0.6–0.9, across the nucleus.

Based on the velocity field and line ratios, H₂ is most likely thermally excited by UV radiation from OB stars. Since [Fe II] is blueshifted in the nucleus and is more extended parallel to the cone than perpendicular to it, [Fe II] is likely to be shock-excited by the winds in the cone. In the NE peak shocks also seem to contribute to the Br γ emission.

No 2–1 S(1) is detected, and the upper limit to the 2–1 S(1)/1–0 S(1) ratio is in agreement with thermal excitation of H₂. Assuming $T_{\text{vib}} = 2000 \text{ K}$, we derive $N_{\text{H}_2} = 3.5 \times 10^{17} \text{ cm}^{-2}$ (corresponding to $M_{\text{H}_2} \simeq 100 M_{\odot}$) within the nuclear aperture. The integrated mass of the excited hydrogen is 200 M_{\odot} parallel to the cone and 160 M_{\odot} perpendicular to it. The FWHM size of the nuclear H₂ emission is similar in both directions (~ 150 pc).

Of the detected coronal lines, [Si VI] 1.964 μm is spatially resolved parallel to the cone (Fig. 3), and is more enhanced toward southwest than northeast. [Si VII] 2.483 μm is also spatially resolved and similarly extended, though its determination suffers from the much higher thermal background noise. The [Si VI] emission within the innermost 2 arcsec is composed of a resolved nuclear source with FWHM ~ 1.6 arcsec (170 pc) and an additional, decaying extended component towards southwest. Furthermore, after subtracting the underlying CO lines, a marginal [Ca VIII] 2.321 μm line appears at a 2.8σ level with flux $0.42 \pm 0.15 \times 10^{-15} \text{ ergs cm}^{-2} \text{ s}^{-1}$.

3.5 NGC 2992

NGC 2992 is a nearby ($z = 0.00771$; distance = 30.6 Mpc) almost edge-on peculiar Sa galaxy with a Sy2 nucleus, interacting with NGC 2993 at 2.9 arcmin (26 kpc) distance toward SE. A prominent dust lane roughly N-S along the major axis of the galaxy splits the nuclear region into two components. NGC 2992 has an unusually extensive cone emerging almost perpendicularly from the plane of the galaxy up to ~ 4 kpc (~ 25 arcsec) distance in SE-NW direction (Allen et al. 1999), with the SE cone brighter than the NW cone. The radio structure of NGC 2992 has major axis PA = 160°, with a one-sided extension along PA = 130°, and at smaller scales a “figure of 8” shape at PA = 160° (e.g. Ulvestad & Wilson 1984).

The *H*- and *K*-band spectra of NGC 2992 are shown in Fig. 2 and Fig. 8. The strongest emission line in the nucleus is the broad Br γ 2.166 μm . Other nuclear lines are [Fe II] 1.644 μm , He I 2.058 μm , coronal lines and various H₂ lines, including 2–1 S(1) 2.248 μm . NGC 2992 has been previously observed spectroscopically in the *JHK*-bands in January 1999 also with SOFI and 1 arcsec slit by Gilli et al (2000). Compared to them, the emission lines have become brighter and Br γ much broader (2530 km s^{-1}) than their Pa α . Furthermore a relatively strong [Al IX] line at 2.043 μm has appeared.

The most extended line is 1–0 S(1), which can be traced up to 7 arcsec (1.1 kpc) distance perpendicular to the cone but only up to 1 arcsec (220 pc) parallel to it. Both Br γ and [Fe II] are more extended (~ 4 arcsec; 600 pc) parallel to the cone than 1–0 S(1). In addition, toward southwest H₂

Table 4. The mass and the column density of the excited H₂ in the nucleus (1.4 arcsec aperture), the nuclear spatial size corrected for the seeing (FWHM; Section 2) and the integrated H₂ mass within the starforming regions and the nuclear spatial extent of the lines, both parallel to the cone (\parallel) and perpendicular to it (\perp). The nuclear extent given in parsecs is in the plane of the galaxy and other values are in the plane of the sky. The integrated masses and the spatial extents are given over the whole galaxy for NGC 4945 and NGC7582. Star \star indicates that the central peak is significantly off-nuclear.

Nucleus	1068 Sy2	1097 Sy1	1365 Sy1.8	1386 Sy2	1566 Sy1	2110 Sy2	E428 Sy2	2992 Sy2	3081 Sy2	3227 Sy1.5	3783 Sy1	4945 Sy2	5128 Sy2	7582 Sy2
Paper	II	I	II	I	I	II	II	II	II	I	II	I	I	II
Broad Br γ	no	...	yes	yes	yes	yes	no	yes	no	yes	yes	no	no	yes
M(H ₂) [M $_{\odot}$]	1800	25	<60	17	42	250	100	500	110	280	290	55	32	220
N(H ₂) [10 ¹⁷ cm ⁻²]	130	1.5	<2.1	3.7	1.9	4.3	3.5	8.8	1.8	22	3.2	80	44	7.8
M(H ₂) \parallel [M $_{\odot}$]	2200	90	90	50	90	220	200	350	80	310	290	70	30	320
M(H ₂) \perp [M $_{\odot}$]	2100	60	290	30	110	190	160	560	160	350	270	150	30	480
FWHM H ₂ \parallel [pc]	...	99	...	<20	65	320	140 \star	120	210	58	...	28	42	...
FWHM H ₂ \perp [pc]	...	108	...	39	82	230	150	250	160	84	...	57 \star	35	...
FWHM [Fe II] \parallel [pc]	100 \star	<20	<30	220	160 \star	80	...	50	130	50	<10	310
FWHM [Fe II] \perp [pc]	80	<20	<30	100	130	140	...	40	<100	50	<10	160
Extent H ₂ \parallel ["]	5.4	3.0	...	4.2	2.0	4.5	4.9	1.0	1.5	6.0	0.6	17	10	2.3
Extent H ₂ \perp ["]	4.1	0.9	...	1.0	2.9	1.5	1.5	6.7	1.0	7.5	0.6	36	16	6.7
Extent [Fe II] \parallel ["]	3.2	0.8	0.5	4.1	2.8	1.0	0.6	1.6	0.6	4.8	1.2	1.9
Extent [Fe II] \perp ["]	5.4	0.8	0.5	1.9	1.9	6.2	0.6	2.0	0.6	7.2	1.2	3.6
Extent Br γ \parallel ["]	5.4	...	3.0	0.8	0.5	...	2.3	1.9	1.9	2.3	1.0	3.1	1.1	1.9
Extent Br γ \perp ["]	2.3	...	4.0	0.8	1.1	...	1.0	2.3	0.6	1.3	0.6	7.8	0.6	3.2
Extent H ₂ \parallel [pc]	450	340	...	410	210	730	530	470	240	600	130	1600	240	580
Extent H ₂ \perp [pc]	320	80	...	190	280	300	270	1300	200	860	130	1200	720	720
Extent [Fe II] \parallel [pc]	270	80	50	660	300	480	90	160	130	420	30	480
Extent [Fe II] \perp [pc]	420	150	50	380	340	1200	120	230	130	230	50	390
Extent Br γ \parallel [pc]	450	...	590	80	50	...	250	900	250	230	220	270	30	480
Extent Br γ \perp [pc]	180	...	430	150	100	...	180	450	120	150	130	250	30	340
T_{vib} [10 ³ K]	<5.3	<2.6	...	<2.5	<2.7	3.3	<2.6	2.6	<2.3	2.0	<4.8	2.2	<1.8	2.9

emission is detected associated with the bridge connecting NGC 2992 to NGC 2993. This emission is likely to be shock-excited, as 2–1 S(1) emission is not detected. There are also separate Br γ regions perpendicular to the cone 5 arcsec (760 pc) from the nucleus, coinciding with the bar or spiral arms (Fig. 1).

The velocity field of NGC 2992 is shown in Fig. 5. The velocity curve of [Fe II] is blueshifted by 70 km s⁻¹. However, the velocity curve of Br γ seems to follow more closely H₂ than [Fe II].

The 1-0 S(1)/Br γ ratio is quite low, 0.28, suggesting thermal UV heating. The [Fe II]/Br γ ratio is 0.93 and [Fe II]/Br γ_{narrow} = 16. Considering that [Fe II] is blueshifted in the nucleus, it is plausible that [Fe II] is excited by shocks. The narrow Br γ emission may also originate in shocks, as the narrow Br γ /1–0 S(1) ratio is \sim 0.2, but as Br γ is kinematically more closely coupled with H₂ than [Fe II], the shocked regions producing Br γ are not likely to coincide with [Fe II] regions. In addition to Br γ , also He I is broad (2200 km s⁻¹) (Fig. 7).

The dereddened 2–1 S(1)/1–0 S(1) ratio 0.18 (corresponding to T_{vib} = 2600 K) is in agreement with thermal excitation of H₂. The density of the excited molecular hydrogen is N_{H_2} = 8.8 \times 10¹⁷ cm⁻², corresponding to integrated gas mass of \sim 500 M $_{\odot}$. The FWHM size of the nuclear H₂ emission is smaller parallel to cone (120 pc) than perpendicular to it (250 pc).

Three coronal lines ([Si VI] 1.964 μ m, [Si VII] 2.483 μ m and [Al IX] 2.043 μ m) are detected in NGC 2992. In addition, there appears to be a fairly broad (80 Å) [Ca VIII] 2.321 μ m

line detected at 2.5 σ level. The coronal lines are weaker than those in NGC 1068 and NGC 3081 (this paper), and it is not possible to discuss whether the lines are spatially resolved.

3.6 NGC 3081

NGC 3081 is a nearby (z = 0.00795; distance = 31.6 Mpc) Sy2 galaxy with four rings (e.g. Buta & Purcell 1998), a large-scale bar at PA = 66°, and a nuclear bar at PA = 120° (Storchi-Bergmann et al. 1996). H α imaging shows a ring of H II regions with major axis perpendicular to the large-scale bar (Storchi-Bergmann et al.).

The H - and K -band spectra of NGC 3081 are shown in Fig. 2 and Fig. 8. The coronal lines [Si VI] 1.964 μ m and [Si VII] 2.484 μ m are by far the strongest emission lines detected in the nuclear region. Also the coronal [Ca VIII] 2.321 μ m and [Al IX] 2.043 μ m lines, various H₂ 1–0 S- and Q-transition lines, He I 2.058 μ m, narrow Br γ , and a weak [Fe II] 1.644 μ m are detected.

The most extended line is [Si VI] followed by Br γ and 1–0 S(1) 2.122 μ m, which both extend \sim 2 arcsec (310 pc; Fig. 3). Br γ , 1–0 S(1) and [Fe II] are very narrow, comparable to the instrumental width of the lines (\sim 30–32 Å). Also [Fe II] is not spatially resolved.

The [Fe II]/Br γ ratio is 0.64, one of the lowest in the sample, and can be produced by star formation. The 1–0 S(1)/Br γ ratio is 1.6, indicating shocks as excitation mechanism also for H₂. The upper limit to the nuclear 2–1 S(1)/1–0 S(1) ratio is 0.13, while the 1–0 S(0)/1–0 S(1) and 1–0 S(2)/1–0 S(1) ratios are 0.13 and 0.57, respectively, clearly

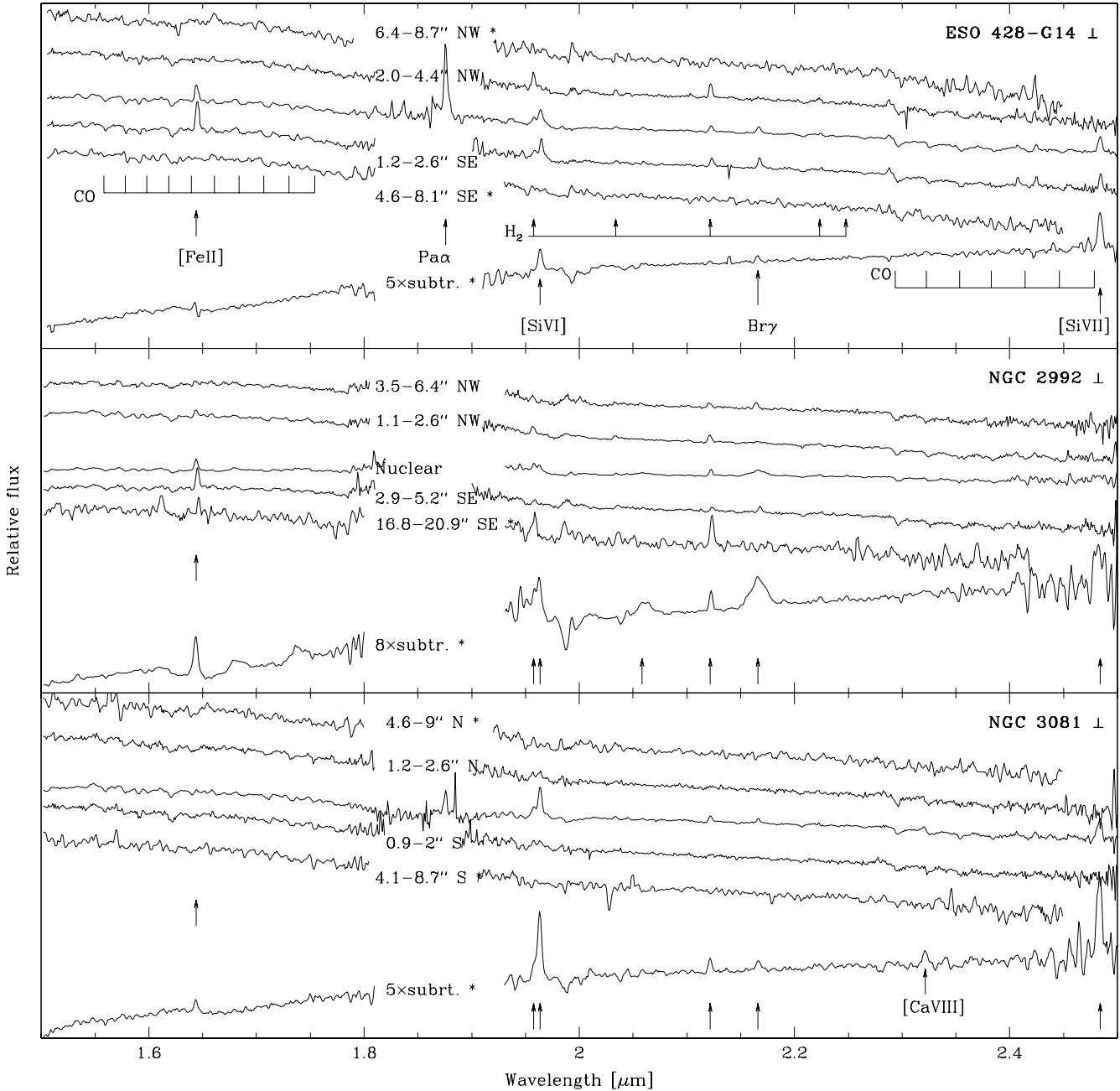


Figure 8. The 1.5–2.5 μm spectra of ESO 428-G14 (*top*), NGC 2992 and NGC 3081 (*bottom*) perpendicular to the cone at different positions along the slit. For symbols, see Fig. 4.

ruling out UV fluorescence, and suggesting shocks to be responsible for the excitation of H_2 . In the nuclear 1.4 arcsec aperture, the gas density $N_{\text{H}_2} = 1.8 \times 10^{17} \text{ cm}^{-2}$, corresponding to gas mass of only $110 M_{\odot}$. The FWHM size of the nuclear H_2 emission is larger parallel to the cone (210 pc) than perpendicular to it (160 pc). The integrated mass of excited H_2 is $80 M_{\odot}$ parallel to the cone and $70 M_{\odot}$ perpendicular to it.

In contrast with the other galaxies in the sample with circumnuclear rings (e.g. NGC 1097, NGC 1365 and NGC 4945), the rings in NGC 3081 are not prominent in the spec-

tra. The effective slit length covers only the nuclear ring (PA \sim 120 $^\circ$; major axis \sim 12 arcsec; 1.9 kpc) and partially the inner ring (\sim 75 $^\circ$; 70 arcsec; 11 kpc). In the nuclear ring, Br γ 2.166 μm is only visible after smoothing the spectra, and no emission lines from the inner ring can be detected.

The coronal [Si VI] line is more extended parallel to the cone (FWHM 2.2 arcsec; 350 pc) than perpendicular to it (1.2 arcsec; 200 pc). Perpendicular to the cone the emission peak is slightly off-nuclear. This extended emission cannot be detected in the [Si VII] line due to the much higher background noise this line suffers.

3.7 NGC 3783

NGC 3783 is an (R')SB(r)a galaxy with a Sy1 nucleus. It is the most distant ($z = 0.00973$; distance = 38.6 Mpc) galaxy in our sample, but one of the closest Sy1s, and thus has been extensively studied (e.g. Maran et al. 1996). It has an inner ring (diameter ~ 35 arcsec; 6.7 kpc) with star formation activity circling a strong stellar bar (PA = 163°), and thin tightly wound spiral arms emerging from this ring (e.g. Mulchaey et al. 1997). NGC 3783 has extremely broad Balmer and He lines which are blueshifted relative to the systemic velocity (Evans 1988).

Non-stellar continuum appears to dominate the overall spectrum of NGC 3783 (Fig. 9). The strongest line within the nuclear aperture is the broad (~ 2630 km s $^{-1}$) Br γ . Other lines detected are 1–0 S(1), [Fe II], He I, *H*-band Brackett lines and three coronal lines. Similarly to the case of NGC 3081, NGC 3783 is rather distant and faint and each line can only be traced up to ~ 1 arcsec (200 pc) from the nucleus (Fig. 10). Thus, no kinematical analysis can be presented for NGC 3783.

Similarly to the case of NGC 2992, in addition to broad Br γ , a faint broad He I line is detected (Fig. 2). This line also appears to be double-peaked in contrast to Br γ (Fig. 7). The width of He I (~ 3700 km s $^{-1}$) is broader than that of Br γ , and the peaks are separated by ~ 1000 km s $^{-1}$. In the *H*-band, other Brackett transition lines are detected (Br 10–4 1.737 μm , Br 11–4 1.681 μm and Br 12–4 1.641 μm). Their ratios against Br γ indicate that the BLR is unobscured.

The upper limit to the 2–1 S(1)/1–0 S(1) ratio is ~ 0.3 ($T_{\text{vib}} < 4800$ K), while for fluorescent emission the expected ratio is ~ 0.5 . Thus we cannot exclude the contribution from fluorescent H $_2$ emission. The density of the excited H $_2$ in the nucleus $N_{\text{H}_2} \simeq 3.2 \times 10^{17}$ cm $^{-2}$ (corresponding to $M_{\text{H}_2} \simeq 290 M_\odot$).

Three coronal lines are detected in NGC 3783: [Si VI] 1.964 μm , [Ca VIII] 2.321 μm and [Si VII] 2.483 μm . [Si VI] and [Si VII] are both spatially resolved in the nucleus but no additional extended emission is detected. The FWHM size of the nuclear emission source (corrected for the instrumental resolution) is ~ 0.7 arcsec with no significant difference between the directions. In addition, there appears to be a faint [Al IX] line detected at a 2.5σ level blended with the broad He I line, but higher S/N spectra are required to confirm its presence.

3.8 NGC 7582

NGC 7582 is a nearby ($z = 0.00540$; distance = 20.9 Mpc) (R')SB(s)ab galaxy in the Grus quartet with a Sy2 nucleus. Optical broad-band images (e.g. Malkan, Gorjian & Tam 1998) show a disturbed morphology with an optically obscured nucleus, a red star forming ring (diameter 2 arcsec) and a dust lane crossing the nuclear region. In the NIR, the galaxy appears smoother, and in the *L*-band the nucleus dominates albeit the ring remains visible (Prieto, Reunanen & Kotilainen 2002). Optical spectropolarimetry does not reveal a hidden BLR (Heisler et al. 1997), and even hard X-ray emission is attenuated by large column density (Warwick et al. 1993), indicating that an edge-on torus blocks even the scattered light from the nucleus. However, the nuclear emission is variable, and the broad hydrogen recombination line

has been detected by Sosa-Brito et al. (2001). The sharp-edged [O III] outflow cone of NGC 7582 (PA = 250°) was detected by Storchi-Bergmann & Bonatto (1991).

The *H*- and *K*-band spectra are shown in Fig. 9. The strongest nuclear line is Br γ , while the other lines detected are 1–0 S(1) and other H $_2$ lines, [Fe II] and an unidentified emission feature at 2.195 μm , which remains visible after subtracting the continuum. Br γ can be decomposed into broad (~ 3000 km s $^{-1}$) and narrow (420 km s $^{-1}$) components (Fig. 7). The broad component has an additional blue wing and is therefore not perfectly fitted by a simple two-component fit. Two coronal lines ([Si VI] and [Si VII]) are also detected.

1–0 S(1) is the most extended line (Fig. 10) and is more extended perpendicular to the cone (8 arcsec; 900 pc) than parallel to it (2.5 arcsec; 270 pc). 1–0 S(1) emission declines smoothly, but the effect of the ring on the H $_2$ emission is also notable, especially perpendicular to the cone. The ring is more prominent in Br γ and [Fe II], which are detected parallel to the cone up to 4 arcsec (430 pc) in northeast and 2.5 arcsec in southwest and ~ 2 arcsec perpendicular to the cone. The emission lines are narrow, comparable to or slightly larger than the instrumental resolution. He I is also strong in the ring, in agreement with relatively recent star formation.

The velocity field of NGC 7582 is shown in Fig. 5. Parallel to the cone the velocity curves are relatively flat, and similar for the various emission lines. [Fe II] is systematically blueshifted with respect to H $_2$. The ratio of [Fe II]/narrow Br γ = 3.1 is larger than models predict for star forming regions, but in agreement with shocks or X-rays.

The ratio of 2–1 S(1)/1–0 S(1) = 0.20 ± 0.06 in the nucleus in agreement with thermal excitation of H $_2$ ($T_{\text{vib}} = 2900 \pm 500$ K). Assuming $T_{\text{vib}} = 2000$ K, the density of H $_2$ is 7.8×10^{17} cm $^{-2}$, corresponding to a gas mass of 220 M_\odot . The integrated mass of the excited hydrogen is 320 M_\odot parallel to the cone and 480 M_\odot perpendicular to it across the galaxy. The nuclear H $_2$ emission is too weak to accurately determine the FWHM size of the nucleus.

The coronal lines [Si VI] 1.964 μm and [Si VII] 2.483 μm are weak, and it is not possible to reliably measure the size of the coronal emission region. However, the detection of coronal lines supports the presence of AGN in NGC 7582, as does the detection of broad Br γ .

4 DISCUSSION

We have presented NIR 1.5–2.5 μm long-slit spectra of eight Seyfert galaxies with an ionization cone. Combined with similar data on six Seyferts from Paper I, the total sample size is 14 Seyferts (three Sy1s, two intermediate Seyferts and nine Sy2s). The discussion below is based on this total sample. The strongest emission line is Br γ 2.166 μm in 43 % of the galaxies (two Sy1s, two Sy2s and two intermediate Seyferts), [Fe II] 1.644 μm in 21 % (three Sy2s), 1–0 S(1) 2.122 μm in 14% (one Sy1, one Sy2) and a coronal line (either [Si VI] 1.964 μm or [Si VII] 2.484 μm) in 21 % (three Sy2s). If a broad Br γ line is detected, it is the strongest line in 5/8 (62 %) galaxies, while [Fe II] remains the strongest line in NGC 2110 and NGC 3227 and [Si VII] in NGC 1386.

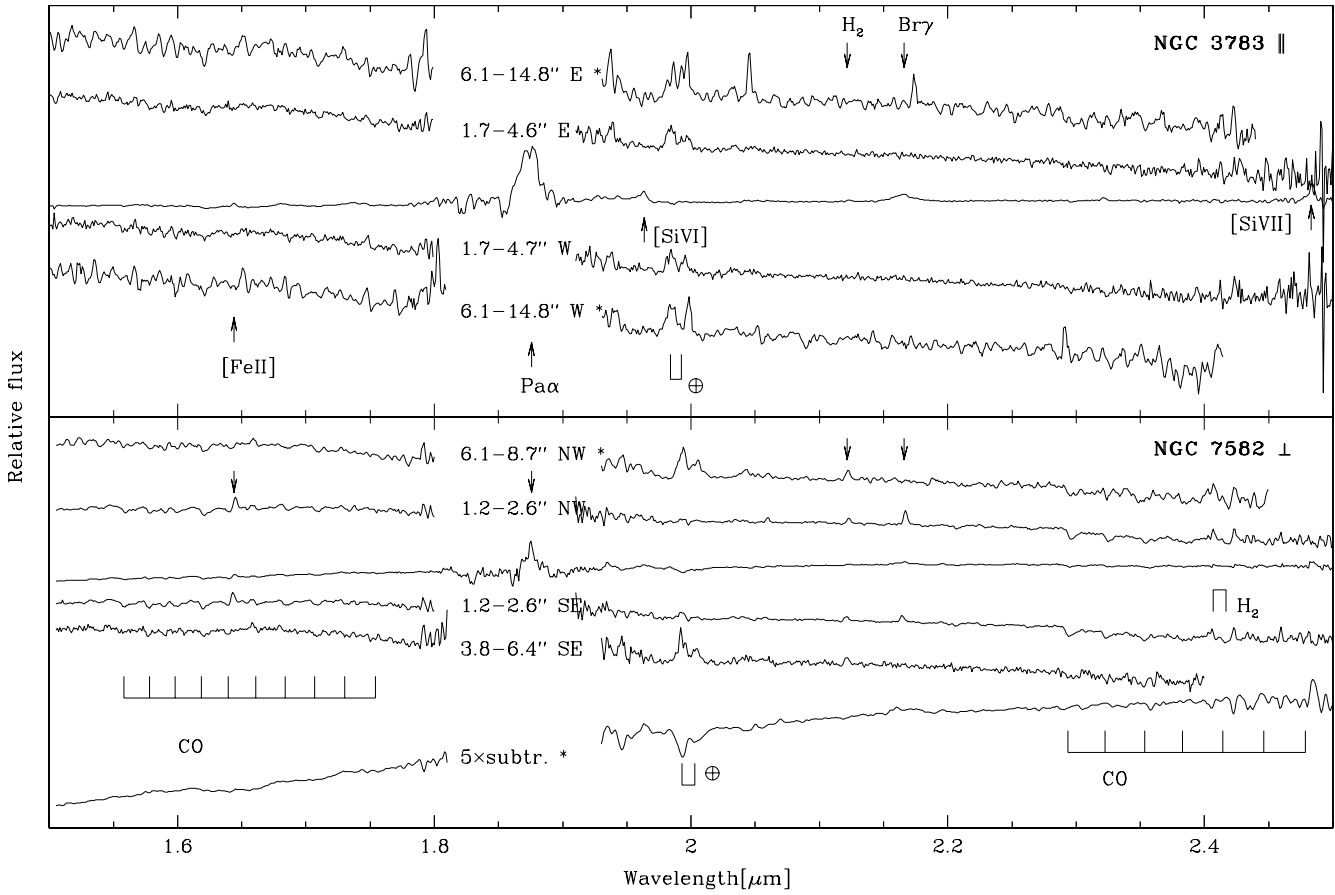


Figure 9. The 1.5–2.5 μm spectra of NGC 3783 (top) and NGC 7582 (bottom) at different positions along the slit. For symbols, see Fig. 4.

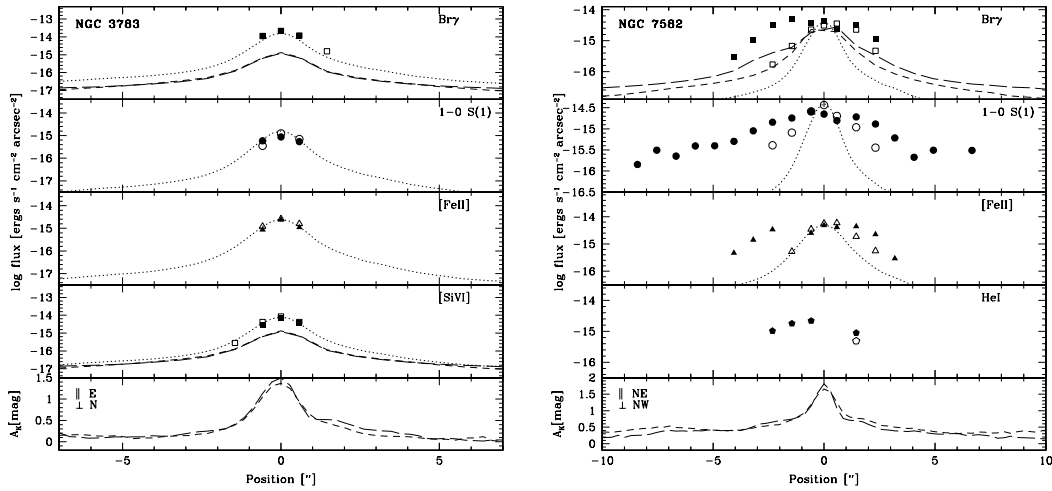


Figure 10. The observed line emission in NGC 3783 (left) and NGC 7582 (right). Symbols are as in Fig. 3.

4.1 Br γ emission

The only galaxy in the sample with no nuclear Br γ 2.166 μm emission is NGC 1097 (Paper I), which we, however, classify in the following discussion as Sy1 based on the literature. Broad nuclear Br γ emission is detected in 8/14 (57 %) galaxies in the sample. Of these galaxies, only two were optically classified as Sy1s and two as intermediate Seyferts, while the remaining four (NGC 1386, NGC 2110, NGC 2992 and NGC 7582) were classified as Sy2s. Two of these galaxies (NGC 1386 and NGC 7582) have no indication of a hidden BLR in polarized light (Tran 2001). The only other galaxy common with Tran's sample is NGC 1068, where BLR region is detected in polarized emission but not in Br γ . The detection of broad Br γ in ~ 40 % (4/9) of the optically classified Sy2s is mainly due to the lower extinction that the nuclear emission suffers in the NIR (Fig 11). The high detection rate of broad Br γ is also a consequence of the high spatial resolution and quality of the data used.

If the classification is based on the detection of Br γ , Sy2 galaxies have larger extinction than Sy1s (Fig. 11). The two Sy2s with low A_K are ESO 428-G14 and NGC 3081, both of which are among the least luminous in the sample, while the three high A_K Sy2 galaxies (NGC 1068, NGC 4945 and NGC 5128) represent the high luminosity end of the sample. Whether the obscuring material is related to the molecular torus or a foreground dust screen is unknown; the latter explanation seems more plausible as the optical depth of the molecular torus is likely to be high enough to completely obscure the BLR. The foreground absorbing material may be in the form of star forming clouds, which are known frequently to coexist with the AGN (e.g. Storchi-Bergmann et al. 2001). This explanation seems likely, as 75 % (6/8) of the galaxies which have broad Br γ also have a narrow component. Alternatively narrow Br γ may arise from the NLR.

Additionally, in two galaxies (Sy1 NGC 3783 and Sy2 NGC 2992) broad He I 2.058 μm emission was detected. In both of them, the width of He I is comparable to that of Br γ , and the broad dereddened He I/Br γ flux ratio ~ 0.35 . One possible explanation for the non-detection of broad He I in most of the sample galaxies is the intrinsic weakness of He I with respect to Br γ , or the atmospherically poor region that He I is located in. The role of extinction seems unlikely as $A_{\text{HeI}} \simeq 1.1A_{\text{Br}\gamma}$.

4.2 [Fe II] emission

Spatially resolved *nuclear* [Fe II] 1.644 μm emission is detected in 57 % of the galaxies (8/14; one Sy1, two intermediate Seyferts, and five Sy2s). In spatially resolved cases, the FWHM size of the nuclear emission corrected for the seeing ranges from 40 pc in NGC 3227 to ~ 300 pc in NGC 7582. The total extent of the nuclear [Fe II] emission ranges from ~ 30 pc in NGC 5128 to 1.2 kpc in NGC 2110, with average extent ~ 300 pc in the plane of the galaxy. In many galaxies *separate* emission regions are detected further out from the nucleus. This extended emission is very patchy, and in most galaxies closely follows the star forming complexes as [Fe II] is fairly correlated with Br γ 2.166 μm and He I 2.058 μm , which both are tracers of star formation. The origin of this extended [Fe II] emission is thus very likely due to star form-

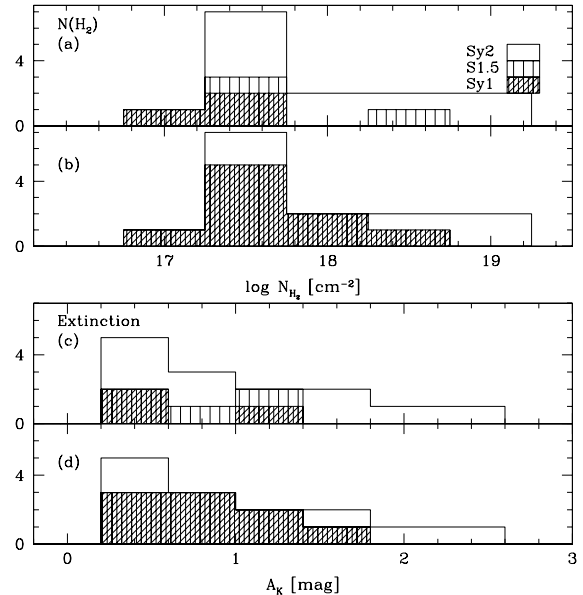


Figure 11. The nuclear surface density of molecular hydrogen (a, b) and the extinction in the nuclear aperture (c, d). The classification in panels a and c is based on literature, and in b and d on the detection of broad Br γ (This paper).

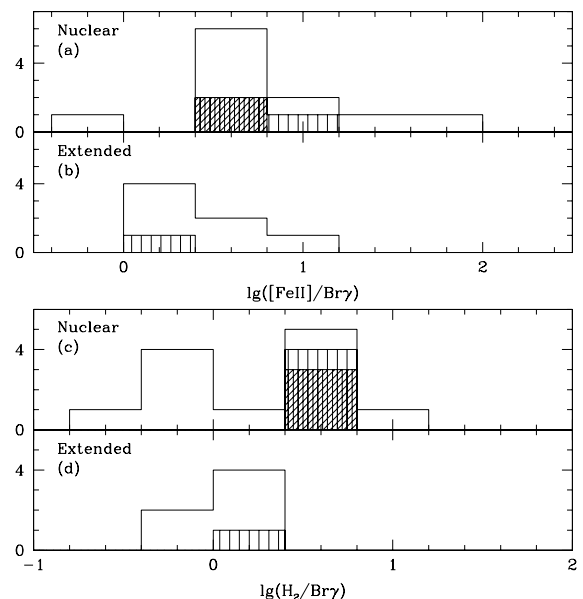


Figure 12. The logarithmic [Fe II]/Br γ_{narrow} ratios (a, b) in the nuclear aperture and for the extended emission, and the $\text{H}_2/\text{Br}\gamma_{\text{narrow}}$ ratios (c, d). The shading is as in Fig. 11.

ing processes and supernovae. The low [Fe II]/Br γ ratios 0.5 – 2 (Fig. 12) of this extended emission are also generally in agreement with theoretical models of star forming regions (e.g. Colina 1993).

The origin of the *nuclear* [Fe II] is however unclear. Recently, Rodriguez-Ardila et al. (2002) studied four narrow-line Sy1 galaxies in the wavelength range 0.8 - 2.4 μm , and

suggested that a combination of collisional excitation and decays from levels populated by Ly photons produce the NIR [Fe II] spectrum. Other suggestions include shocks and X-ray excitation.

The weaker *H*-band [Fe II] lines are too faint to yield reliable line ratios, but the [Fe II]/Br γ ratio is sensitive to the excitation mechanism. However, the Br γ fluxes used in this ratio should exclude the broad component, because the BLR is unlikely to contribute much to the [Fe II] flux. The [Fe II]/Br γ_{narrow} ratios are high in all the galaxies with a broad component, ranging from ~ 3 in NGC 3783 to ~ 80 in NGC 2110 (Fig. 12). These ratios are much higher than star formation models predict, but can be produced by X-ray or shock excitation. Often, the [Fe II] is broader than the instrumental profile, reaching up to FWHM ~ 700 km s $^{-1}$, and blueshifted with respect of Br γ . Both of these are signatures of shock excitation. In NGC 1386 and NGC 2110 the spatial correlation between X-ray and [Fe II] emission favours X-ray excitation. In galaxies without broad Br γ the [Fe II]/Br γ ratio is also fairly high, ~ 3 . Only in NGC 3081 this ratio is low, 0.6, obtainable with shocks, photoionization or star formation. Thus the [Fe II] is predominantly excited by shocks produced by winds/jets in the ionization cone.

4.3 H $_2$ emission

Nuclear H $_2$ emission was detected in all galaxies except in NGC 1365. The surface densities of the excited H $_2$ (Table 4) range from 1.5×10^{17} cm $^{-2}$ in NGC 1097 to 1.3×10^{19} cm $^{-2}$ in NGC 1068. The surface densities tend to be larger in Sy2s than in Sy1s (Fig. 11), but the scatter is large. Also, when classification into Seyfert types is based on the detection/non-detection of broad Br γ emission, this relation disappears. This suggests that the optical classification into Seyfert types is largely related to the extinction effects. However, the scatter of N_{H_2} is larger in narrow Br γ galaxies than in broad Br γ galaxies.

The nuclear 1–0 S(1) 2.122 μm emission is spatially resolved in all the galaxies except parallel to the cone in NGC 1386. The FWHM extent of nuclear H $_2$ emission is larger perpendicular to the cone than parallel to it in 6/8 (75 %) galaxies (Fig. 13), while in four galaxies the nuclear H $_2$ emission is too weak to obtain accurate FWHM sizes and in two galaxies the H $_2$ emission center is significantly off-nuclear. The FWHM sizes corrected for the seeing range from < 20 pc in NGC 1386 to ~ 300 pc in NGC 2110, and are larger than the predicted sizes for the molecular torus (1–100 pc; Pier & Krolik 1993). Thus the emission is more likely to arise from the molecular material (disk?) surrounding the torus than directly from the torus itself.

Extended nuclear emission is detected in all the galaxies except in NGC 1386 and NGC 3783. The overall 1–0 S(1) emission is more extended perpendicular to the cone than parallel to it in five galaxies, while the opposite is true in seven galaxies. The extended nuclear 1–0 S(1) emission can be detected up to a range of physical scales in the plane of the galaxy, from ~ 100 pc in NGC 5128 to > 1 kpc in NGC 2992 and NGC 4945. Since this extended nuclear emission declines smoothly with increasing radius, it seems probable that the molecular gas forms a disc surrounding the nucleus. This is further supported by the 1–0 S(1) velocity curves, which are generally well-ordered. A starburst origin for this

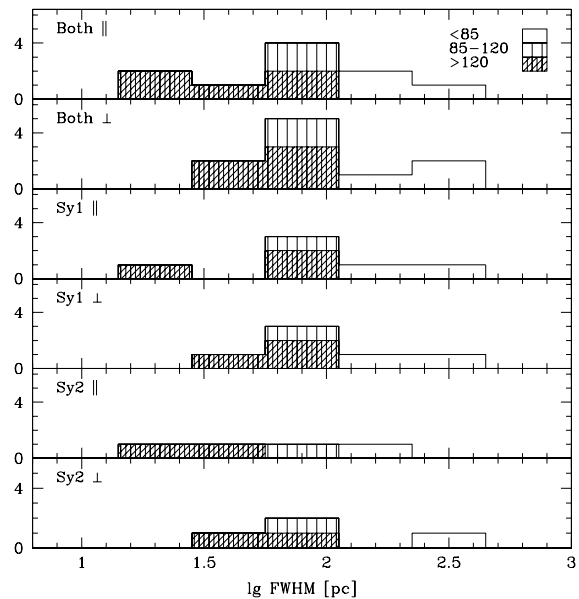


Figure 13. The FWHM size of the H $_2$ emission both parallel to the cone and perpendicular to it for the whole sample (*upper two panels*) and separately for both Sy types (*lower panels*). The classification is based on the detection of broad Br γ . Different physical scales (pc/arcsec) are indicated with shading.

smooth extended emission seems excluded as the morphologies of both Br γ and [Fe II] emission are generally different from that of H $_2$. In seven galaxies, *separate* off-nuclear 1–0 S(1) emission knots are also detected. In most cases these H $_2$ patches are also detected in Br γ and [Fe II] and likely originate from starforming regions. In conclusion, extended H $_2$ emission appears to be related with two main components: the first associated with star forming regions and the second a smoothly decaying disk, which is not observed in [Fe II] or Br γ .

Only in 36 % (5/14) of the galaxies, nuclear 2–1 S(1) 2.244 μm emission was detected and the 2–1 S(1)/ 1–0 S(1) ratio or their upper limits are inconsistent with significant fluorescent excitation, and in agreement with thermal excitation. Furthermore, off-nuclear 2–1 S(1) emission is detected only in two galaxies, and is also consistent with thermal excitation of the molecular H $_2$. This is valid even in the ring of NGC 1365, where the EW of the Br γ 2.166 μm line is ~ 70 Å, indicative of a strong UV radiation field. Whether the thermal excitation is produced by shocks, X-rays or UV fluorescence in dense clouds, remains unclear, although shocks are the most likely explanation.

4.4 Coronal line emission

Four coronal lines were detected: [Si VI] 1.964 μm , [Al IX] 2.043 μm , [Ca VIII] 2.321 μm and [Si VII] 2.4833 μm . Of these lines, [Si VI] was detected in eight, [Al IX] in two, [Ca VIII] in four and [Si VII] in seven galaxies. Overall, at least one coronal line was detected in 57 % of the galaxies (8/14; one Sy1, one intermediate Seyfert and six Sy2s). This substantially increases the number of Seyferts with IR coronal line detection, and confirms the results of Prieto & Viegas (2000),

that coronal lines are common and bright in the spectra of Seyfert galaxies. The [Al IX] line has been detected so far to our knowledge only in Circinus (Maiolino et al. 1998), NGC 2992 and NGC 3081 (this paper). In addition, in a few galaxies either [Ca VIII] or [Al IX] was detected at $\sim 2.5\sigma$ level, and awaits confirmation. Coronal lines are detected in 2/5 galaxies (40 %), where Br γ 2.166 μm is narrow, and in 5/8 galaxies (62 %) where Br γ is broad.

Interestingly, the coronal lines are extended parallel to the cone in all three galaxies with spatial information, i.e. NGC 1068, NGC 3081 and ESO 428-G14, implying an anisotropic nuclear radiation field. In NGC 1068 the extended emission is only visible on one side, in NGC 3081 both sides are similarly extended and in ESO 428-G14 the emission is more extended toward southwest than northeast. Furthermore, in NGC 3783 the coronal lines are spatially resolved, but the size is similar both parallel and perpendicular to the ionization cone. We have an on-going followup program to obtain diffraction limited images of nearby Seyferts in the [Si VII] line to study the coronal line region in detail (Prieto et al. 2003).

5 CONCLUSIONS

Near-infrared 1.5–2.5 μm long-slit spectroscopy with a resolution of $\sim 300 \text{ km s}^{-1}$ of eight nearby Seyfert galaxies is presented. Together with similar data of additional six Seyfert galaxies (Paper I), a homogeneous sample of high quality NIR spectra with a spatial resolution ≤ 1 arcsec is produced both parallel to the ionization cone and perpendicular to it. This dataset allows us to study the spatial extension and kinematics of [Fe II], H $_2$, Br γ and coronal lines, and the sizes of the central emitting regions down to < 0.5 arcsec (10 - 100 pc), and the central molecular content within a 1.4 arcsec diameter aperture. The main results are:

(i) The strongest NIR emission lines in the nuclear spectra are Br γ , H $_2$ 2.12 μm , [Fe II] 1.64 μm and coronal lines [Si VI] 1.96 μm and [Si VII] 2.48 μm .

(ii) Broad Br γ was detected in ~ 40 % of the observed Sy2 galaxies, stressing the importance of extinction effects and classifying AGN in the infrared. The existence of genuine Sy2s on the basis of nondetection of the BLR in polarized emission (Tran 2001) is inconsistent with our detection of broad Br γ in two of the candidates proposed by the author. We instead believe that high spatial resolution NIR spectroscopy will reveal more hidden broad line objects in the future.

(iii) Large concentrations of H $_2$ are present in the nucleus regardless of the Seyfert type. The nuclear surface densities of excited H $_2$ range from 10^{17} to 10^{19} cm^{-2} . In general, two extended components are detected: a smoothly decaying disk and (in some cases) circumnuclear starforming ring. While the ring is prominent also in [Fe II] and Br γ , the disk is only detected in H $_2$.

(iv) According to the unified models the putative torus collimating the radiation from AGN should be evident as more extended nuclear emission perpendicular to the cone than parallel to it. This is indeed detected in 6/8 (75 %) galaxies.

(v) There is a good spatial and kinematical correlation between Br γ and [Fe II]. Generally two components are dis-

tinguished: one related with a circumnuclear ring and a nuclear component. Extended [Fe II] and Br γ emission is detected in half of the sample. Nuclear [Fe II] is in many galaxies blueshifted and the width of [Fe II] reaches up to 700 km s^{-1} FWHM, which together with high [Fe II]/Br γ ratios suggests shock excitation as a dominant excitation mechanism in Seyfert galaxies.

(vi) Coronal lines [Si VI] and [Si VII] are present in ~ 60 % of the objects and also [Ca VIII] and [Al IX] are detected in some cases, confirming the results of Prieto & Viegas (2000) that coronal lines are common and bright features in the spectra of Seyfert galaxies regardless of the type of the nucleus. In three galaxies the coronal lines are extended parallel to the cone but not perpendicular to it. This clearly supports the presence of a strong anisotropic radiation field in these galaxies. However, due to the high ionization potential of the coronal lines, the extended emission cannot be produced by the nuclear ionizing radiation unless it is strongly collimated. Thus shock excitation caused by e.g. the jet interacting with the interstellar medium is the most plausible origin for the extended coronal emission. The width of the coronal lines (up to 1200 km s^{-1}) also supports this scenario.

6 ACKNOWLEDGEMENTS

Based on observations collected at the European Southern Observatory, La Silla, Chile. This research has made use of the NASA/IPAC Extragalactic Database (NED), which is operated by the Jet Propulsion Laboratory, California Institute of Technology, under contract with the National Aeronautics and Space Administration. JR acknowledges a grant from Finnish Cultural Foundation during this work.

REFERENCES

- Allen M.G., Dopita M.A., Tsvetanov Z.I., Sutherland R.S. 1999, ApJ 511, 686
- Alloin D., Galliano E., Cuby J.G., Marco O., Rouan D., Clenet Y., Granato G.L., Franceschini A. 2001, A&A 369, L33
- Antonucci R. 1993, ARA&A 31, 473
- Bergvall N., Johansson L., Olofsson K. 1986, A&A 166, 92
- Black J.H., van Dishoeck E.F. 1987, ApJ 322, 412
- Buta R., Purcell G.B. 1998, AJ 115, 484
- Colina L. 1993, ApJ 411, 563
- Davies R.I., Sugai H., Ward M.J. 1998, MNRAS 300, 388
- Evans I.N., Ford H.C., Kinney A.L., Antonucci R.R.J., Armus L., Caganoff S. 1991, ApJ 369, 27
- Evans I.N. 1988, ApJS 67, 373
- Falcke H., Wilson A.S., Simpson C., Bower G.A. 1996, ApJ 470, 31
- Gilli R., Maiolino R., Marconi A., Risaliti G., Dadina M., Weaver K.A., Colbert E.J.M. 2000, A&A 355, 485
- Gredel R., Dalgarno A., 1995, ApJ 446, 852
- Heisler C.A., Lumnden S.L., Bailer J.A. 1997, Nature 385, 700
- Hollenbach D., McKee C.F. 1989, ApJ 342, 306
- Hunt L., Malkan M.A., Salvati M., Mandolesi N., Palazzi E. 1997, ApJS 108, 229
- Knop R.A., Armus L., Matthews K., Murphy T.W., Soifer B.T. 2001, AJ 122, 764
- Kotilainen J.K., Reunanen J., Laine S., Ryder S. 2000, A&A 353, 834

- Kristen H., Jörsäter S., Lindblad P.O., Boksenberg A. 1997, *A&A* 328, 483
- Landini M., Natta A., Salinari P., Oliva E., Moorwood A.F.M. 1984, *A&A* 134, 284
- Lidman C., Cuby J.-G., Vanzi L. 2000 SOFI User's manual, LSO-MAN-ESO-40100-0003
- Lutz D., Maiolino R., Moorwood A.F.M., Netzer H., Wagner S.J., Sturm E., Genzel R. 2002, *A&A* 396, 439
- Maiolino A., Krabbe A., Thatte N., Genzel R. 1998, *ApJ* 493, 650
- Malaguti G., Bassani L., Cappi M., Comastri A., di Cocco G., Fabian A.C., Palumbo G.G.C., Maccacaro T., et al. 1999, *A&A* 342, 41
- Malkan M.A., Gorjian V., Tam R. 1998, *ApJS* 117, 25
- Maloney P.R., Hollenbach D.J., Tielens G.G.M. 1996, *ApJ* 466 561
- Maran S.P., Crenshaw D.M., Mushotzky R.F., Reichert G.A., Carpenter K.G., Smith A.M., Hutchings J.B., Weymann R.J. 1996, *ApJ* 465, 733
- Marco O., Alloin D. 2000, *A&A* 353, 465
- Moran E.C., Barth A.J., Kay L.E., Filippenko A.V. 2000, *ApJ* 540, L73
- Mulchaey J.S., Wilson A.S., Bower G.A., Heckman T.M., Krolik J.H., Miley G.K. 1994, *ApJ* 433, 625
- Mulchaey J.S., Wilson A.S., Tsvetanov Z. 1996, *ApJ* 467, 197
- Mulchaey J.S., Regan M.W., Kundu A. 1997, *ApJS* 110, 299
- Oliva E., Moorwood A.F.M. 1990, *ApJ* 348, 5
- Peletier R.F. et al. 1999, *ApJS* 125, 363
- Pier E.A., Krolik J.H. 1993, *ApJ* 428, 124
- Prieto M.A., Marco O., Reunanen J., Kotilainen J.K. 2003, under preparation
- Prieto M.A., Reunanen J., Kotilainen J.K. 2002, *ApJ* 571, 7L
- Prieto M.A., Viegas S.M. 2000, *ApJ* 532, 238
- Puxley P.J., Hawarden T.G., Mountain C.M. 1990, *ApJ* 364, 77
- Reunanen J., Kotilainen J.K., Prieto M.A. 2002, *MNRAS* 331, 154 (Paper I)
- Rodríguez-Ardila A, Viegas S.M., Pastoriza M.G., Prato L. 2002, *ApJ* 565, 140
- Rouan D., Rigaut F., Alloin D., Doyon R., Lai O., Crampton D., Gendron E., Arsenault R. 1998, *A&A* 339, 687
- Sandqvist A., Jörsäter S., Lindblad P.O. 1995, *A&A* 295, 585
- Schinnerer E., Eckart A. Tacconi L.J. 2001, *ApJ* 549, 254
- Sosa-Brito R., Tacconi-Garman L.E., Lehnert M.P., Gallimore J.F. 2001, *ApJS* 136, 61
- Sternberg A., Dalgarno A. 1989, *ApJ* 338, 197
- Stevens I.R., Forbes D.A., Norris R.P 1999, *MNRAS* 306, 479
- Storchi-Bergmann T., Bonatto C.J. 1991, *MNRAS* 250, 138
- Storchi-Bergmann T., Rodríguez-Ardila A, Schmitt H.R., Wilson A.S., Baldwin J.A. 1996, *ApJ* 472, 83
- Storchi-Bergmann T., Winge C., Ward M.J., Wilson A.S. 1999, *MNRAS* 304, 35
- Storchi-Bergmann T., Gonzales-Delgado R.M., Schmitt H.R., Cid Fernandes R., Hechman T. 2001, *ApJ* 559, 147
- Thompson R.I., Cham R.-R., Corbin M.R., Epps, H. 2001, *ApJ* 558, L97
- Tran H.D. 2001, *ApJ* 554, L19
- Ulvestad J.S., Wilson A.S. 1984, *ApJ* 285, 439
- Ulvestad J.S., Wilson A.S. 1989, *ApJ* 343, 659
- Veilleux S., Goodrich R.W., Hill G.J. 1997, *ApJ* 477, 631
- Warwick R.S., Sembay S., Yaqoob T., Makishima K., Ohashi T., Tashiro M., Kohmura Y. 1993, *MNRAS* 265, 412
- Weaver K.A., 2001, in "The central kpc of starbursts and AGN: the La Palma connection", Eds. J.H. Knapen, J.E. Beckman, I. Shlosman and T.J. Mahoney, ASP conf. series, vol. 249, 389
- Wilson A.S., Baldwin J.A. 1989, *AJ* 98, 2056
- Winge C., Storchi-Bergmann T., Ward M.J., Wilson A.S. 2000, *MNRAS* 316, 1
- Wolniewicz L., Simbotin I., Dalgarno A. 1998, *ApJS* 115, 293